SCIENCE CHINA
Technological Sciences

•Review•

March 2022 Vol.65 No.3: 493–518
https://doi.org/10.1007/s11431-020-1800-8

Twin-roll strip casting of advanced metallic materials

ZHU ChenYang[1,2,3], ZENG Jie[1,2] & WANG WanLin[1,2*]

[1] *School of Metallurgy and Environment, Central South University, Changsha 410083, China;*
[2] *National Center for International Research of Clean Metallurgy, Central South University, Changsha 410083, China;*
[3] *Department of Materials Science and Engineering, Faculty of Engineering, National University of Singapore, Singapore 117576, Singapore*

Received December 13, 2020; accepted February 25, 2021; published online December 15, 2021

Metallic materials have historic and served as critical enablers of human progress, wealth, and wellbeing over millennia. Recently, the global demand for the development of environment-friendly and energy-saving technology has been increasing, with the aim to support the sustainability of metallic materials. Twin-roll strip casting (TRC) is one of the most cutting-edge technologies and a near-net-shape manufacturing method in the steel industry, which conforms to the green fabrication trend of next-generation high-performance metallic materials. By utilizing the dominant characteristics of sub-rapid solidification, and integration of solidification, solid-state transformation, and deformation; TRC has become a meaningful way to deal with the most challenging issues in the processing of metallic materials, and made a significant contribution to materials manufacturing. Hence, we review the TRC process of various metallic materials, including plain carbon steels, stainless steels, Fe-Si electrical steels, high-strength steels, clad steels, aluminum alloys, magnesium alloys, metallic glasses, and so on. This paper offers an outlook of future opportunities for various advanced metallic materials development through the TRC process, and inspires more in-depth research.

twin-roll strip casting, metallic materials, steels, alloys

Citation: Zhu C Y, Zeng J, Wang W L. Twin-roll strip casting of advanced metallic materials. Sci China Tech Sci, 2022, 65: 493–518, https://doi.org/10.1007/s11431-020-1800-8

1 Introduction

Metallurgical technology has been crucial to the development of the world and its economy, and metallic materials have served as critical enablers of human progress, wealth, and wellbeing over millennia [1,2]. The design and development of new types of metallic materials are dependent on the advancement of metallurgy technology.

Recently, the global demand for environment-friendly and energy-saving technology has been increasing, with the aim to support the sustainable development of metallic materials [3]. Twin-roll strip casting (TRC) is one of the most cutting-edge technologies and a near-net-shape manufacturing method in the steel industry. The initial idea of TRC was conceived by Bessemer in 1856 [4]. TRC can produce thin strips with a thickness of 1–2 mm directly from liquid metal, reducing or eliminating the following rolling steps. It fully conforms to the green fabrication trend of next-generation high-performance metallic materials and can provide an opportunity to shorten the material manufacturing process. TRC process also owns advantages of high efficiency, high quality, and energy-saving, which would greatly benefit the sustainability of modern industry [5].

The schematic illustration of the layout of the CASTRIP facility at Nucor, one of the most typical and successful TRC projects, is shown in Figure 1 [6]. Before casting, the tundish, transition piece, side dam, and other refractory materials need to be preheated. In the process of casting, the molten steel begins with the ladle and successively flows through the tundish, transition piece, and core nozzle to the melt pool

* Corresponding author (email: wanlin.wang@gmail.com)

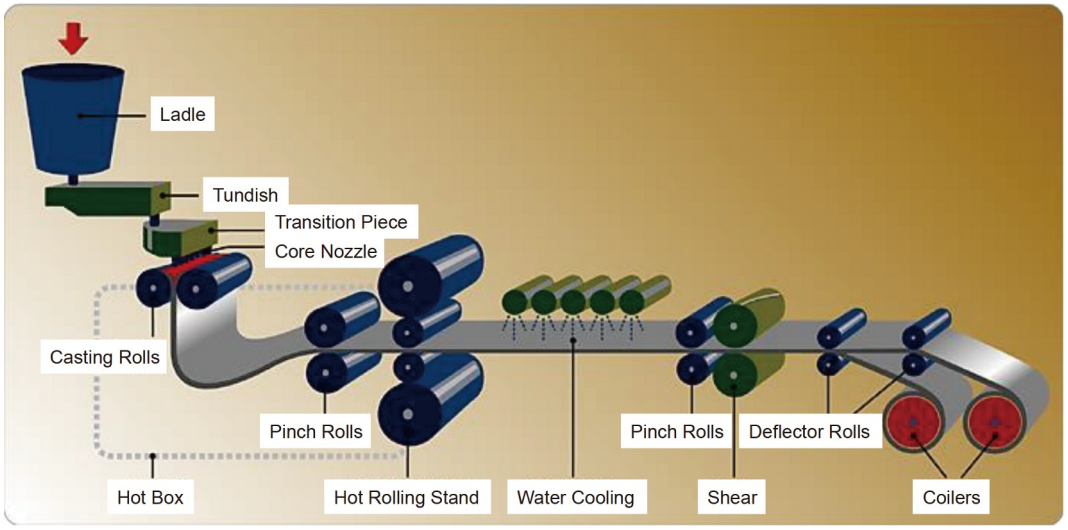

Figure 1 (Color online) The schematic illustration of the layout of the CASTRIP facility at Nucor. Reprinted with permission from ref. [6], Copyright © 1969, Springer Science Business Media, Inc.

formed by the side dam and casting rolls. High-speed cooling water is fed into the casting rolls, and the molten steel gradually solidifies on the surface of the rolls. When passing through the rolls gap, the casting rolls squeeze the solidified shells on both sides into a strip of certain thickness. Then, the strip is transmitted to the pinch roll, from which it is fed into the hot rolling mill. After rolling the strip to a target thickness, it is cooled to a target temperature by a water-cooling system and enters into a coiler for coiling.

During the TRC process, the shells and casting rolls travel rotationally in intimate contact down through the melt pool, unlike the conventional continuous casting process where the mold is oscillated to facilitate withdrawal of the slab. Furthermore, the solidification fundamentals of the TRC process are greatly different as compared to conventional or thin-slab continuous casting. The casting parameters for the CASTRIP process compared to conventional continuous casting are shown in Table 1 [6].

The cooling rate can reach range from 10^2 to 10^4 K/s during TRC in general, which belongs to the sub-rapid solidification process [7]. By utilizing the dominant characteristics of sub-rapid solidification, and integration of solidification, solid-state transformation, and deformation; TRC has become a meaningful way to deal with the most challenging issues that occurred in the traditional casting process, including elements segregation, inclusions precipitation, non-uniform solidification, and microstructure coarsening, etc., in the processing of metallic materials.

Since the beginning of the 21st century, TRC has contributed to materials manufacturing (Figure 2). It has attracted numerous world-famous universities and institutions devoted to the studies of TRC, e.g., Carnegie Mellon University [4], Max Planck Institute [8], McGill University [9], Seoul National University [10], Tohoku University [11], Nippon Steel Corporation [12], University of Sydney [13], RWTH Aachen University [14], Shanghai Jiao Tong University [15], Northeastern University [16], Central South University [17], and Chinese Academy of Sciences [18], etc.

As well, many kinds of steels, including plain carbon steels [8], stainless steels [19], Fe-Si electrical steels [16], high-

Table 1 The casting parameters for the CASTRIP process compared to the conventional continuous casting [6]

Parameter	CASTRIP process	Thin slab casting	Conventional slab casting
Strip thickness (mm)	1.6	50	220
Casting speed (m/min)	80	6	2
Total solidification time (s)	0.15	45	1070
Shell cooling rate (°C/s)	1700	50	12

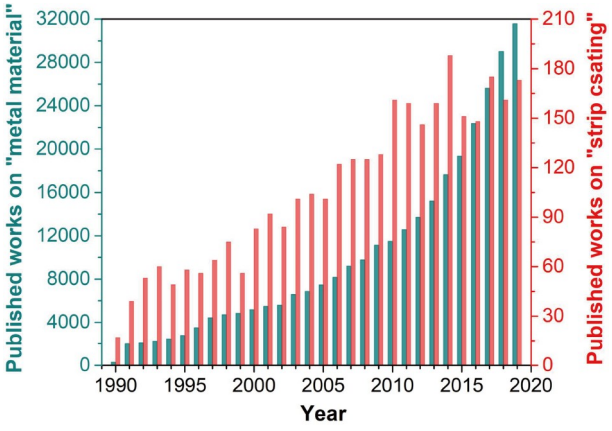

Figure 2 (Color online) Number of published works on "metal material" and "strip casting" (from 1990 to 2019, search on Web of Science).

strength steels [14], clad steels [20]; non-ferrous metallic materials, including aluminum alloys [21], magnesium alloys [22], metallic glasses [18], and other alloys or composites have been studied or manufactured through TRC process (Figure 3).

Until now, only very few review papers have been published related to TRC technology. Zapuskalov [23] conducted a comparative review paper between the TRC and the conventional continuous casting process; Ge et al. [9,24] and Maleki et al. [25] reviewed the historical and technical developments of TRC. There is no published review regarding the TRC process of metallic materials to the present authors' best knowledge. Yet, sharply increasing types of metallic materials have been involved in the studies of TRC. Therefore, an extensive review work has been conducted regarding the TRC process of various metallic materials, with the aim to offer an outlook of the future opportunities in the TRC process of advanced metallic metals, and inspire more in-depth research.

2 Steels

Steels are the most widely used and consumed metallic materials in economic society, due to their excellent mechanical properties, formability, recyclability, and relatively low production cost [26]. It has been occupying a vital role in modern industrial and agricultural production. Around 1500 BC, artificial iron products firstly appeared on the Anatolian plateau; even today, human society still heavily relies on steel as an essential material basis [27]. In 2019, the global production of crude steels reached 1.87 billion tons [27]. It is tough to imagine what our world would be like without steel.

TRC technology is playing an increasingly crucial role in the area of steel processing. It can significantly shorten the traditional production process and gradually become a new direction for steels' green manufacturing. The plain carbon steels, stainless steels, Fe-Si electrical steels, high-strength steels, and other steels involved in the TRC process studies are discussed in the following sections.

2.1 Plain carbon steels

Plain carbon steels are still the most widely used metallic materials globally, due to their low cost, good formability, and mechanical properties that can meet most engineering structures' demands. The TRC process of plain carbon steel started at the end of the 20th century [28]. However, there are only several published studies regarding plain carbon steels, which might be due to these steels are lack of outstanding performance to meet the increasing requirement of modern industry.

The casting parameters, surface quality, and mechanical properties of strip products are the critical issues in the research of the TRC process of carbon steels. Guillet et al. [28] revealed the mechanical properties of the 1008 as-cast strips were inferior to those of industrial hot bands because of the presence of Widmannstatten microstructure (Figure 4(a)). Fortunately, the mechanical properties falling within the range of commercial quality steel could be enhanced, if an appropriate rolling and annealing treatment could be added after TRC.

Tavares et al. [29] measured the instantaneous heat transfer behavior at the interface between the rolls and the melt on a pilot twin-roll caster in the casting process of low carbon steels (Figure 4(b)). The result showed that the heat transfer behavior could dramatically influence the as-cast structure, strip quality, and production limitation.

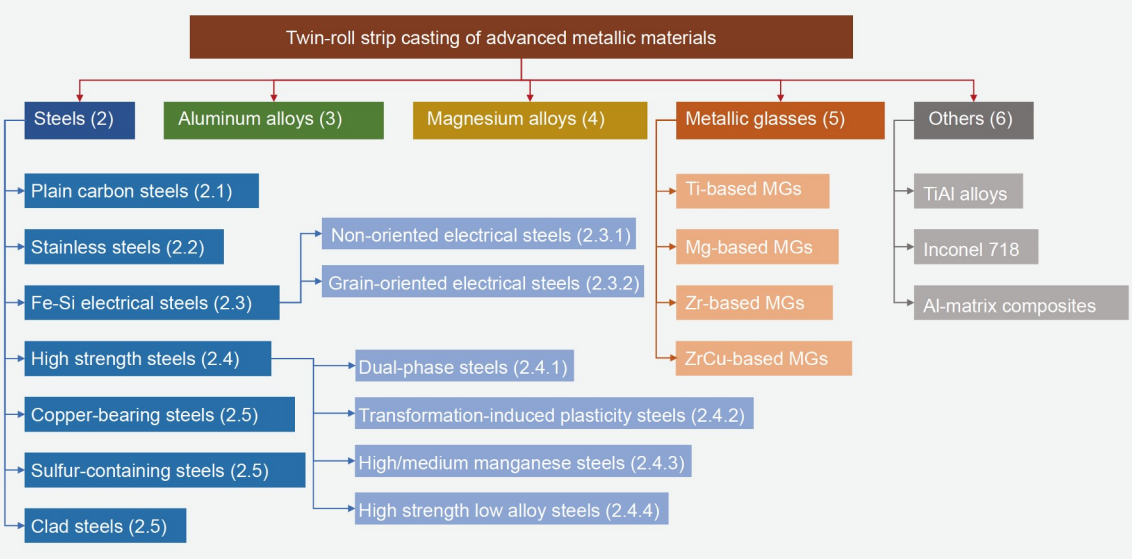

Figure 3 (Color online) Major types of metallic materials produced by TRC in this paper.

2.2 Stainless steels

Containers, pipes, valves, and pumps are always in contact with corrosive media and usually tend to fail due to the metal/media corrosion phenomena [30]. Stainless steels are workhorse materials for our society due to their excellent anti-corrosion capability, and have been used in diverse vital sectors such as petroleum, chemical, and fertilizer industries [31]. They can be roughly divided into three types based on their microstructure at ambient temperature: the austenitic stainless steels, ferritic stainless steels, and duplex stainless steels (DSSs).

Compared with the TRC process of carbon steel, there are more reports about the TRC process of stainless steel [12]. In the earlier studies, 304 stainless steel was the most popular type, and one of the critical issues was surface quality, particularly the surface cracking phenomena occurred during the casting process [32]. The work of Choo et al. [33] showed the cracking phenomenon was directly related to inhomogeneous solidification. Ha et al. [34] found that the microcrack phenomenon was caused by the formation of a black oxide layer during the casting process, which prevents interfacial heat transfer and leads to uneven stress cracking.

Hunter and Ferry [35,36], and Liu et al. [37] studied the microstructure and texture evolution behaviors of ferritic and austenitic stainless steel during the TRC process. They found that ⟨001⟩ oriented grains had an exceedingly high volume fraction. The essential findings indicated TRC has excellent potential for producing grain-oriented Fe-Si electrical steels.

It should be mentioned that some simulators (dip tester, droplet solidification technique, etc.) were invented for the simulation of the sub-rapid solidification condition during the TRC process, and were used in the research of TRC of stainless steels in the 20th century. This equipment has been improved in recent years (Figure 5) [15,38–41]. The simulators made the casting parameter studies more convenient; also, they provided new research methods of TRC for designing new types of steels.

High-performance stainless steels were studied in recent years, such as DSSs, super-austenitic stainless steels (SASSs), and high borated stainless steels.

DSSs are advanced stainless steels composed of austenite and ferrite. They effectively combine the advantages of single ferrite and austenite structure with good mechanical properties. At the same time, they have good corrosion resistance, especially chloride stress corrosion cracking resistance, compared to austenitic 304 or 316. TRC process owns a rapid cooling rate that could effectively control the microstructure and phase evolution of DSSs [41]. Furthermore, subsequent cold-rolling and annealing could optimize their mechanical properties. Zhao et al. [42] successfully produced a TRIP-aided lean DSS strip with good tensile strength (1000 MPa) and excellent high elongation (65%).

SASSs are known for their excellent toughness and corrosion resistance, which are guaranteed by the high content of alloying elements. Segregation behavior is more likely to occur when the alloying elements are at a high level. The TRC process has shown considerable superiority for controlling element segregation and secondary phase precipitation behaviors in the processing of SASSs [43]. The work of Hao et al. [44] indicated that the alloying elements in the as-cast TRC strips were more evenly distributed than conventional ingot (Figure 6), and the mechanical properties of the strips were generally better than those produced by the conventional process.

High-boron stainless steel is a new type of austenitic stainless steel modified with 1.5–2.25 wt% B element. It has outstanding corrosion resistance and thermal neutron absorption performance, so it has a good application prospect in the nuclear power industry. However, large network borides formed in the traditional continuous casted steels' microstructure would seriously damage their hot workability and mechanical properties. In contrast, the as-cast microstructure obtained from the TRC process was ultra-fine, and most borides were smaller than 5 μm without network-like distribution (Figure 7(a)–(c)) [45]. After hot rolling and solution treatment, the strip had excellent mechanical properties (Figure 7(d)). The result provided a potential solution for

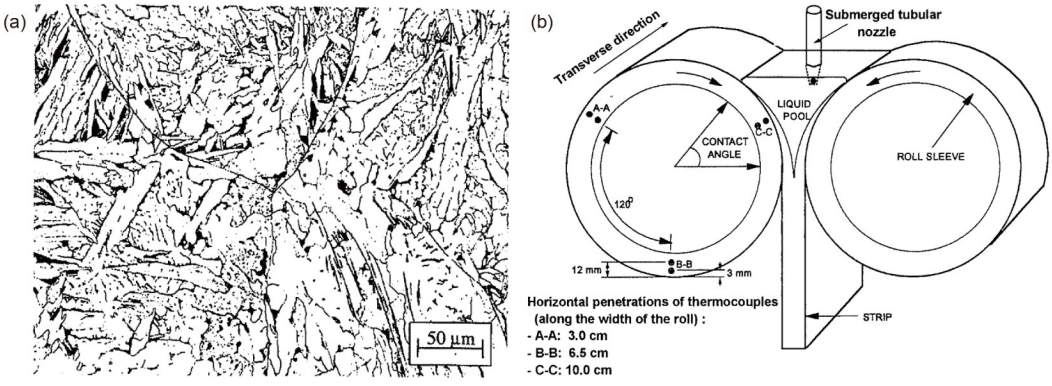

Figure 4 TRC process of plain carbon steels. (a) Widmannstatten microstructure in the as-cast 1008 strip [28]; (b) pilot twin-roll caster [29].

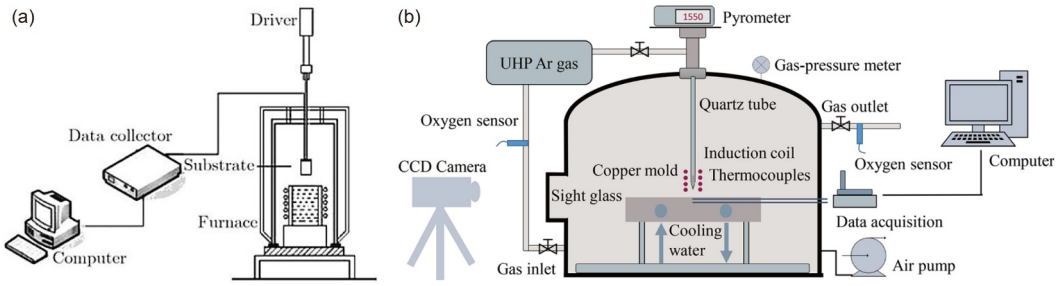

Figure 5 (Color online) Schematic of equipment for the simulation of TRC. (a) Dip tester [15]; (b) droplet solidification technique [41]. (a) Reprinted with permission from ref. [15], Copyright © 2011, Shanghai Jiaotong University and Springer-Verlag Berlin Heidelberg.

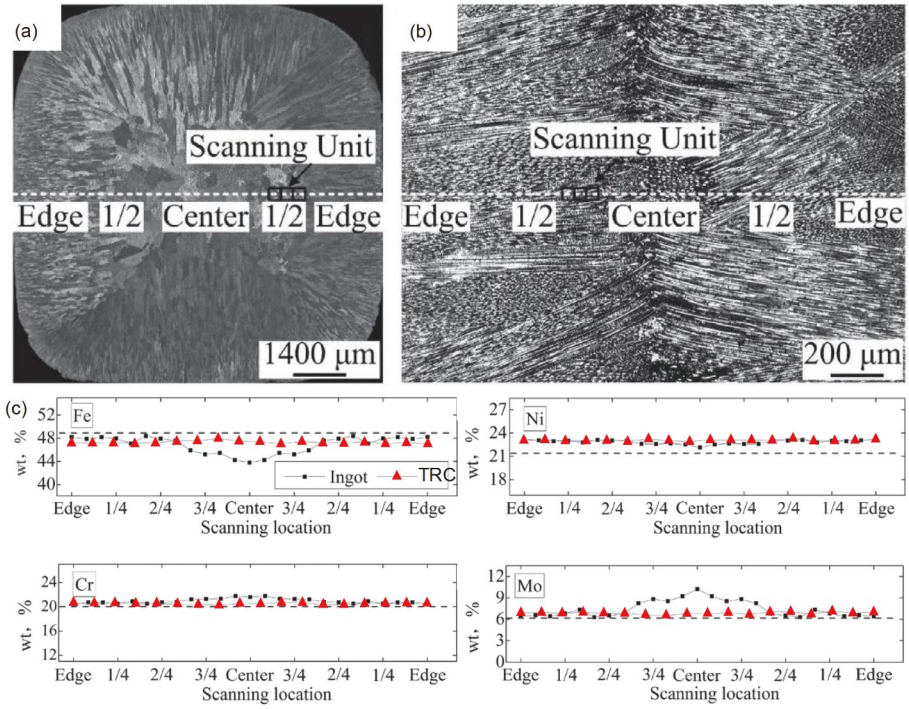

Figure 6 (Color online) Segregation behavior in SASS [44]. (a) Macro solidification structures of the ingot with the conventional process; (b) macro solidification structures of the as-cast TRC strip; (c) elements distribution in the as-cast structures.

the treatment of the brittle second phase in metallic materials processing.

In short, the TRC process of stainless steel is more successful than the case of plain carbon steel, and some stainless steel produced by TRC shows good mechanical properties.

2.3 Fe-Si electrical steels

Fe-Si electrical steels are necessary soft magnetic materials and are widely used in motors, transformers, electronic equipment, and other fields [46]. According to their structure and texture, silicon steels can be divided into non-oriented electrical steel (NOES) and grain-oriented electrical steel (GOES).

2.3.1 Non-oriented electrical steels

NOES have excellent magnetic properties (e.g., high permeability, low core loss, etc.) and consume millions of tons per year [47]. The electric motor's stator and rotor cores are usually made of NOES, which reduces the motor's noise and energy consumption [48]. NOES' crystal structure and texture play the most critical role in their magnetic properties [49]. The key to obtaining excellent magnetic properties such as high magnetic induction and low core loss is to improve the {100} texture intensity and control the optimal grain size of NOES products [50].

Intense dynamic recrystallization often occurs in the hot rolling stage in the conventional process, which leads to grain refinement and affects texture distribution. Refined grains increase grain boundaries and impair the magnetic properties of NOES [16]. Furthermore, it is challenging to manufacture a 6.5 wt% Si NOES strip with a large scale by the traditional method, due to the limited ductility and formability of NOES with high silicon content [51]. However, the solidification structure and grain orientation of NOES could be controlled effectively in the TRC process.

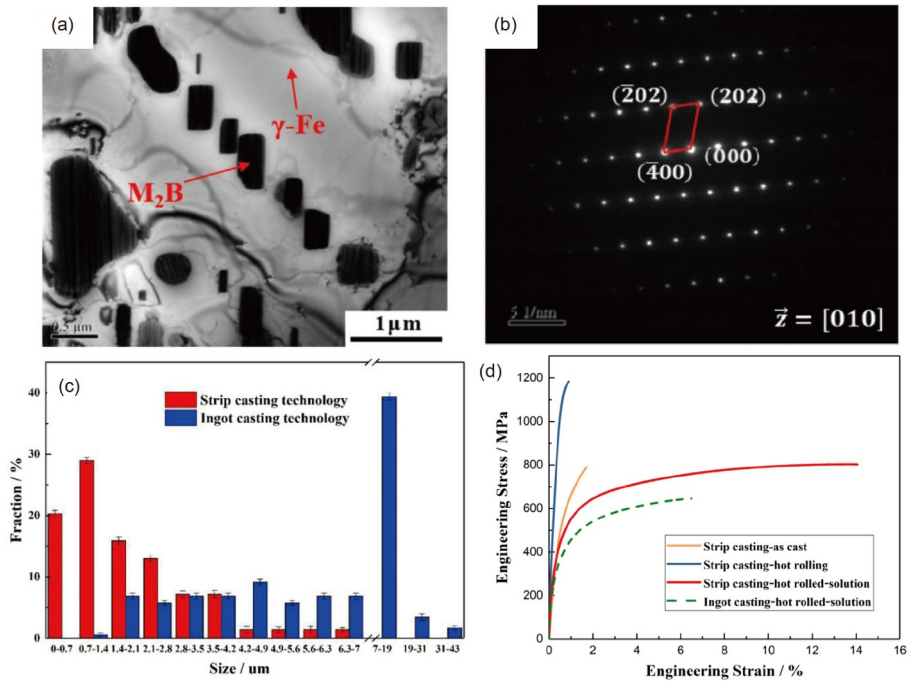

Figure 7 (Color online) High borated stainless steels produced by TRC [45]. (a) Transmission electron microscopy (TEM) image of the microstructure; (b) selected area diffraction pattern (SADP) from the borides; (c) size distribution of the borides; (d) tensile curves of the steels. Reprinted with permission from ref. [45], Copyright © 2019 Elsevier B.V. All rights reserved.

On the other hand, the TRC process can significantly reduce rolling deformation, and it has apparent advantages in producing 6.5 wt% Si NOES [52].

Many studies have been carried out on the TRC process of NOES with Si content ranging from 0.7 to 6.5 wt%. After the TRC process, it usually goes through hot rolling, warm rolling, cold rolling, annealing, and other processes to obtain the tailored microstructure, texture, and magnetic properties. Among these processes, rolling and annealing have a significant impact on the magnetic properties of NOES.

The rolling temperature has a considerable influence on the microstructure, texture, and magnetic properties. Liu et al. [53] found that with increasing rolling temperature from 150°C to 850°C, iron loss and magnetic induction intensity decreased (Figure 8(a), (b)). The study of Chen et al. [54] suggested the hot rolling temperature increased from 950°C to 1050°C can result in a lower core loss, due to the coarse recrystallization microstructure and strong λ fiber texture. However, some studies implied that as the hot rolling temperature changes, magnetic induction and iron loss did not decrease or increase monotonically, but were highly dependent on the hot rolling structure [55]. And the average grain size was usually reduced with the increase of hot rolling reduction (Figure 8(c)) [56]. Conversely, the average grain size after annealing increased with increasing the hot rolling reduction; the anisotropy of grains was improved, and the magnetic induction and iron loss were optimized.

Pre-annealing before cold rolling has an essential effect on the microstructure and magnetic properties of the NOES strip. After pre-annealing, there are many large sizes of precipitated phases in the matrix, which enhance the recrystallization texture of {100} and reduce the core loss significantly [57]. Also, hot band annealing has a considerable effect on NOES. The study of Wang et al. [58] showed that lots of AlN and MnS particles with an average diameter of 57 nm were precipitated during the annealing process (Figure 9(a)–(c)). The precipitated phase's overall volume was much larger than that of the hot-rolled state, which further resulted in the average grain size significantly larger than that of NOES without hot-rolled annealing. The result indicated that hot rolling annealing was an appropriate way to improve the magnetic properties. As well, the heating rate of final annealing had a significant influence on the recrystallization behavior of NOES, and a rapid heating rate was beneficial to optimize the structure and texture (Figure 9(d)) [59].

Coiling temperature is also crucial to the whole process of TRC of NOES. Liu et al. [60] indicated that a higher coiling temperature could significantly improve the recrystallization microstructure, texture, and magnetic properties of NOES. The coiling effect was similar to that of conventional hot band normalizing.

Here, the magnetic properties of the above-discussed NOESs produced by TRC are summarized in Table 2 for reference.

2.3.2 *Grain-oriented electrical steels*

The general Si content in GOES is about 3 wt%, and GOES

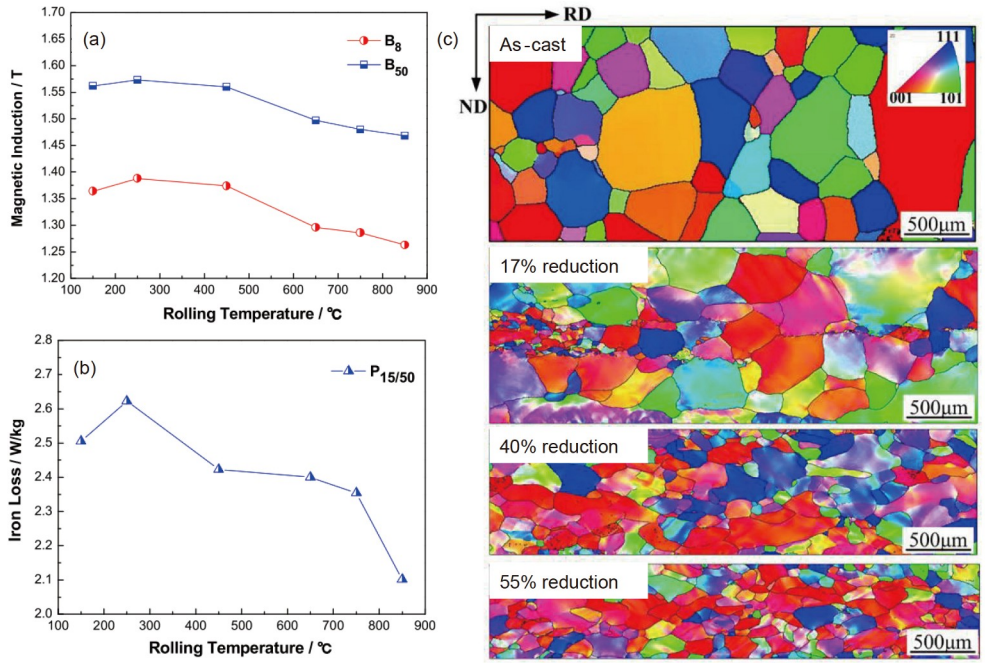

Figure 8 (Color online) Effect of rolling on the NOES. (a) Effect of rolling temperature on the magnetic induction of finally annealed strips [53]; (b) effect of rolling temperature on the iron loss of finally annealed strips [53]; (c) orientation image maps of strips with different hot rolling reductions [56]. (a) Reprinted with permission from ref. [53], Copyright © 2015 Elsevier B.V. All rights reserved. (b) Reprinted with permission from ref. [56], Copyright © 2018 Elsevier B.V. All rights reserved.

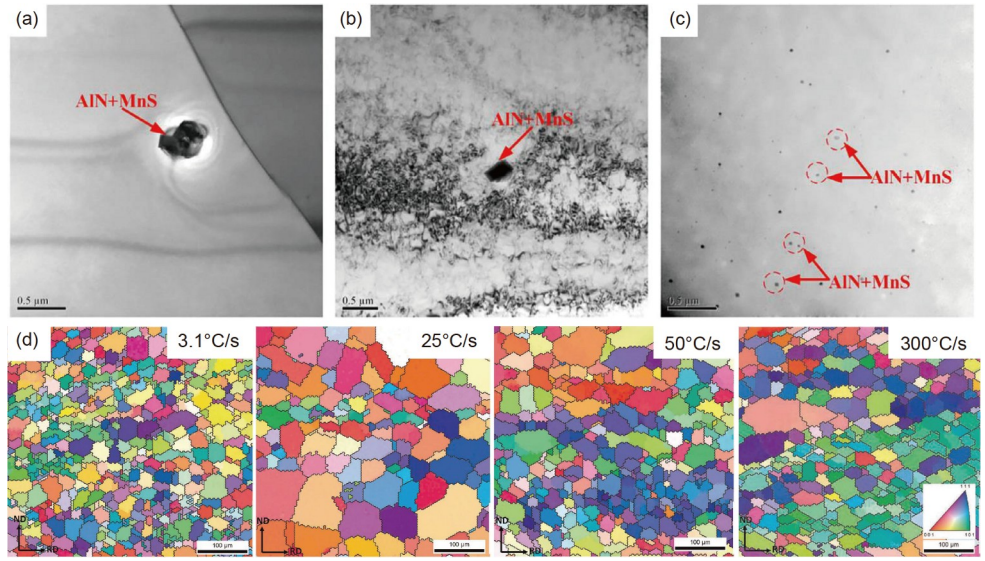

Figure 9 (Color online) Effect of annealing on the NOES. (a) TEM images of precipitates formed in the as-cast strip; (b) hot-rolled strip; (c) hot-rolled and annealed strip [58]; (d) crystal orientation maps of recrystallization grains at different heating rates [59]. (a)–(c) Reprinted with permission from ref. [58], Copyright © 2018 Elsevier B.V. All rights reserved. (d) Reprinted with permission from ref. [59], Copyright © 2015 Elsevier B.V. All rights reserved.

is also an essential soft magnetic material and often used in transformers and other equipment. The strong {110}⟨001⟩ grain orientation (Goss texture) in microstructure plays a significant role in its magnetic properties [61,62].

Although there have been many studies on the production process of GOES, the low cost and high-efficiency production method of high-quality GOES is not yet mature, and further elegant research is still needed [63]. Recently, the TRC process development has provided a new possibility for the production of GOES [64].

It is known that Goss texture is generally caused by shear deformation in the hot rolling stage. The study of Song et al. [65] showed that although the initial solidification structure was different, it was gradually refined with the increasing of hot-rolled reduction, and the hot-rolled coarse-grained strip with 50% reduction showed a more robust Goss texture.

Table 2 Summary of magnetic properties of NOESs produced by TRC[a)]

Si content (wt%)	Thickness (mm)	B_8 (T)	B_{25} (T)	B_{50} (T)	$P_{15/50}$ (W/kg)	$P_{10/50}$ (W/kg)	$P_{10/400}$ (W/kg)	Ref.
0.71	0.5	–	–	1.806	5.69	–	–	[60]
0.71	0.5	–	–	1.785	4.544	–	–	[55]
0.75	0.5	–	–	1.79	4.74	–	–	[54]
1.22	0.5	–	–	1.78	4.9	–	–	[16]
1.23	0.5	–	–	1.803		–	–	[59]
1.3	0.35	–	–	1.83	4.1	–	–	[52]
1.43	0.5	–	–	1.77	4.4	–	–	[16]
2.6	0.35	–	–	1.745	2.92	–	–	[50]
2.6	0.5	–	–	1.735	3.26	–	–	[57]
3.2	0.35	–	–	1.712	3.88	–	–	[58]
6.5	0.3	1.42	–	–	–	0.645	11.51	[47]
6.5	0.3	1.34	1.44	1.54	–	1.01	13.6	[49]
6.5	0.5	1.41	1.50	1.59	–	1.22	21.7	[51]
6.5	0.5	1.39			–	–	24.5	[48]
6.5	0.5	1.383	1.484	1.571	–	–	19.11	[49]

a) B_8, magnetic induction at 800 A m^{-1}; B_{25}, magnetic induction at 2500 A m^{-1}; B_{50}, magnetic induction at 5000 A m^{-1}; $P_{15/50}$, iron loss at 1.5 T, 50 Hz; $P_{10/50}$, iron loss at 1 T, 50 Hz; $P_{10/400}$, iron loss at 1 T, 400 Hz.

Their work also revealed the symmetrical and asymmetrical hot rolling had a significant impact on the microstructure and texture [66]. After symmetric hot rolling, GOES had strong {001}⟨0vw⟩ fiber texture in the outer layer with mild γ-fiber texture formed in the inner layer. However, after asymmetric hot rolling, there were a considerable proeutectoid ferrite and pearlite distributed in the microstructure; Goss texture was stronger, and {001}⟨0vw⟩ fiber texture was stronger in the outer layer.

Several new TRC processing routes, including one or more subsequent hot rolling, normalizing, cold rolling, and annealing were developed in recent years. Cold rolling is the most critical process among these new routes [67]. Due to the lack of sufficient shear deformation, only a small amount of Goss texture was observed in the hot-rolled strip, and sometimes no Goss texture was observed, as most Goss textures originated from the first cold rolling stage [68]. The microstructure was further refined and homogenized during cold rolling or annealing. Finally, it showed a well-developed secondary recrystallization microstructure characterized by sharp Goss grains. Besides, two-stage or three-stage cold rolling was a useful way to acquire suitable microstructure and texture. A completely secondary recrystallized GOES strip with Goss texture was obtained by a new method of TRC combined with the three-stage cold rolling [67].

Fang et al. [69] studied the influence of unconventional cold rolling direction on GOES. The result showed that the completely secondary recrystallization occurred with different rolling inclinations after the final annealing process. The GOES had good magnetic properties when the rolling inclinations were 0° and 90°. Besides, the dynamic strain-aging (DSA) behavior was observed during the warm rolling process (200°C–400°C) [70]. It suggested that the warm rolling process optimized the structure and improved the magnetic properties.

Wang et al. [71] studied the effect of annealing on the texture evolution of GOES produced by the TRC process. They found a lot of particles precipitated during the annealing process, which hindered the crystal rotation during cold rolling. Also, abnormal growth of Goss texture grains and significant improvement of magnetic properties were observed (Figure 10(a), (b)). It is well known that inhibitors

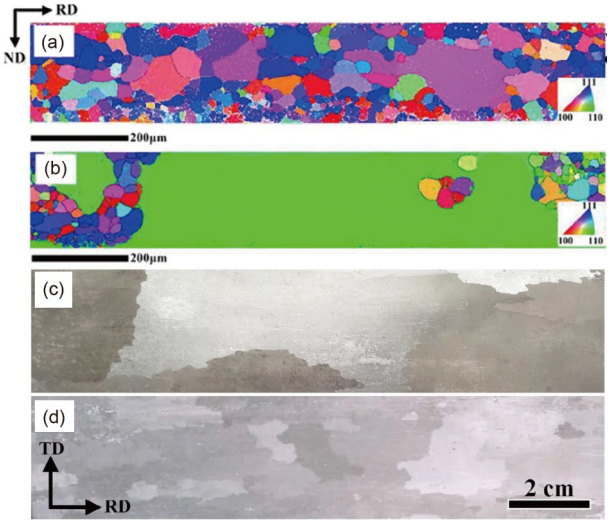

Figure 10 (Color online) Effect of annealing after casting and NbN inhibitor on the GOES. (a) Orientation image map of the secondary annealed strip without annealing; (b) with annealing [71]; (c) macrostructure of the secondary recrystallization strip of Nb-GOES; (d) regular-GOES [72]. (a), (b) Reprinted with permission from ref. [71], Copyright © 2015 Elsevier Inc. All rights reserved. (c), (d) Reprinted with permission from ref. [72], Copyright © 2017 Elsevier B.V. All rights reserved.

play a crucial role in influencing Goss's texture evolution by inhibiting normal grain growth. Fang et al. [72] showed that NbN could be used as an effective inhibitor in GOES. During the secondary recrystallization annealing process, Nb-containing GOES experienced complete abnormal grain growth (Figure 10(c), (d)), which resulted in enhanced magnetic induction.

It is worth mentioning that some research works were conducted on the GOES with high Si content of 4.5 or even 6.5 wt%, and have obtained high Si GOES with excellent magnetic properties [73].

Lu et al. [74] found the GOES strips with Si content of 4.5 wt% had similar magnetic induction and lower core losses than the GOES with 3.0 wt% Si and NOES. Compared with the previously reported 6.5 wt% Si NOES, the prepared 4.5 wt% Si GOES showed superior performance and better processability [75]. Also, the high-frequency core loss of 6.5% wt% Si GOES with adequate secondary grains produced by TRC was significantly lower than that of 6.5 wt% Si NOES and 3.0 wt% Si GOES (Figure 11) [76]. The result indicated that TRC technology was an appropriate route to fabricate GOES with Si content of 3.0, 4.5, and 6.5 wt%.

Here, the magnetic properties of the above-discussed GOESs produced by TRC are summarized in Table 3 for reference.

It can be concluded that various Fe-Si electrical steels have been produced by TRC. Although some processing routes include complicated steps of the rolling and annealing process, it still achieves an excellent performance of electrical steels.

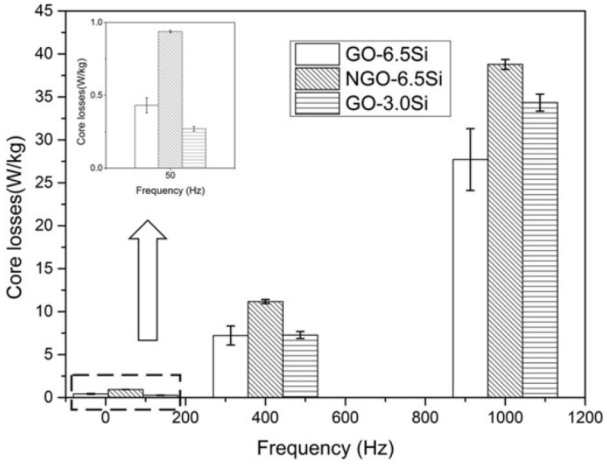

Figure 11 Core loss of the GOES produced by TRC [76]. Reprinted with permission from ref. [76], Copyright © 2017 Elsevier Inc. All rights reserved.

2.4 High-strength steels

In recent decades, high-strength steel has been regarded as the most promising automotive material due to its excellent mechanical properties [26]. It also has been applied in the key components for load-bearing and pressure-bearing in many industrial fields such as metallurgy, mining, machin-

Table 3 Summary of magnetic properties of GOESs produced by TRC[a)]

Si content (wt%)	Thickness (mm)	B_8 (T)	$P_{17/50}$ (W/kg)	$P_{10/400}$ (W/kg)	$P_{10/1000}$ (W/kg)	Ref.
2.85	0.2	1.88	1.6	–	–	[72]
2.9	0.08	1.98	0.7	5.2	20.3	[63]
2.9	0.15	1.88	1.38	–	–	[70]
2.9	0.2	1.84	1.41	–	–	[69]
2.9	0.2	1.84	1.5	–	–	[72]
2.97	0.23	1.94	1.3	–	–	[62]
3.0	0.23	1.79	–	–	–	[71]
3.0	0.23	1.85	–	9.86	40.0	[74]
3.2	0.05	1.72	2.05	8.62	28.16	[68]
3.2	0.1	1.81	1.66	9.64	32.95	[68]
3.2	0.1	1.79	–	6.9	–	[67]
3.2	0.15	1.84	1.78	7.97	29.43	[68]
3.31	0.23	1.84	–	–	–	[61]
3.32	0.27	1.85	1.43	–	–	[64]
4.5	0.2	1.75	–	10.21	42.37	[73]
4.5	0.23	1.73	–	7.80	31.4	[74]
4.5	0.23	1.707	–	8.79		[75]
6.5	0.2	1.76	–	8.659	32.24	[73]
6.5	0.2	1.65	–	–	–	[76]

a) B_8, magnetic induction at 800 A m^{-1}; $P_{17/50}$, iron loss at 1.7 T, 50 Hz; $P_{10/400}$, iron losses at 1 T, 400 Hz; $P_{10/1000}$, iron losses at 1 T, 1000 Hz.

ery, electric power, shipbuilding, and national defense.

For a decade, mounts of studies have been conducted on the TRC process of high-strength steels. Dual-phase steels (DP steels), transformation-induced plasticity steels (TRIP steels), high/medium manganese steels, and high strength low alloy steels (HSLA steels) are the most widely studied types.

2.4.1 Dual-phase steels

DP steel has been widely used in the automobile industry due to its good continuous yield performance, high strength, high strain hardening rate, low yield stress-tensile strength ratio, and good formability. It usually has a high tensile strength in the range of 500–1200 MPa and 12%–34% elongation, and the mechanical properties mainly depend on the ferrite, martensite, and bainite content in the microstructure [77].

Xiong et al. [78] studied the microstructure and properties of DP steel produced by the TRC process. They found that the structure was composed of polygonal ferrite (40%–90%), martensite, a small amount of bainite, and Widmanstatten ferrite, with the tensile strength of 461–623 MPa and 10%–31% elongation. Unfortunately, the as-cast strips' mechanical properties were lower than those of hot-rolled strips due to ferrite, coarse martensite, and Widmanstatten ferrite formed in the microstructure. Whereas they further found that the deformation process can improve the mechanical properties of as-cast strips [79]. After deformation of 17%–46% at 1050°C, static recrystallization resulted in the prior austenite grain refinement, accelerating the ferrite formation and grain refinement, which further improved the mechanical properties. The deformation introduced mechanical properties improvement was mainly ascribed to dislocation and refinement strengthening.

Their study also found that the strain-induced ferrite could increase the strength with a slight reduction of plasticity. The deformation temperature greatly influenced the formation of strain-induced ferrite (Figure 12(a)) [80]. By utilizing the strain-induced ferrite, they obtained a strip through dip test with mechanical properties that reached the level of commercial DP 600. It should be noticed that the strength could be further enhanced by the addition of alloying elements [81].

Recently, Wang et al. [82] successfully prepared a DP steel strip using the TRC process, with the annealed structure composed of 51%–77% martensite, whose tensile strength was around 851–914 MPa, and elongation was of 11%–16% (Figure 12(b)). Further tempering treatment would reduce martensite hardness, leading to a reduction of the tensile strength (702–518 MPa) but an increase of elongation (19.8%–30%) (Figure 12(b)).

2.4.2 Transformation-induced plasticity steels

TRIP steel is generally composed of polygonal ferrite, bainite, martensite, and retained austenite (RA) with good strength and plasticity. TRIP steel is known for its "TRIP effect", which is the transformation from RA to martensite through deformation induction. The TRIP effect can improve its formability, plasticity, and energy absorption ability.

Compared with the traditional hot rolling, cold rolling, and annealing process, the TRC process is a more economical and environmentally friendly method to produce TRIP steel [83]. A TRIP steel strip was prepared by a sub-rapid solidification simulation device combined with a Gleeble 3500 thermo-mechanical simulator [84]. The microstructure was composed of polygonal ferrite (55%), bainite, RA, and martensite (Figure 13(a), (b)), and the mechanical properties were comparable to the commercial TRIP690 thin strip.

Besides, Wang et al. [85] successfully produced a TRIP steel strip through the new process route consisting of TRC, heat treatment, cold rolling, and annealing. The as-cast microstructure was composed of ferrite and martensite (Figure 13(c), (d)). The final annealing microstructure was composed of ferrite and RA (Figure 13(e), (f)), with the tensile strength and elongation reaching 945 MPa and 28.56%.

Xiong et al. [86] conducted an interesting study on the RA in TRIP steel produced by dip tester. The result showed that

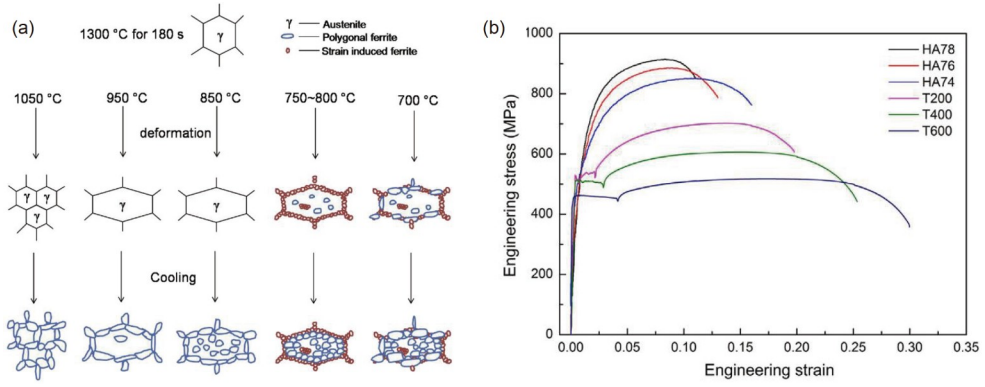

Figure 12 (Color online) DP steel produced by TRC. (a) Schematic diagram of ferrite formation after different deformation temperatures [80]; (b) engineering stress-engineering strain curves [82]. (a) Reprinted with permission from ref. [80], Copyright © 2017 Elsevier Inc. All rights reserved. (b) Reprinted with permission from ref. [82], Copyright © 2017 Elsevier B.V. All rights reserved.

film RA's carbon content was not always higher than that of blocky RA. The RA's carbon content was related to the neighboring phases; sometimes, the blocky RA's carbon content was higher than that in the film or island RA. This work provided crucial theoretical support for tailoring the microstructure of TRIP steel.

2.4.3 High/medium manganese steels

As a candidate material for the new generation of automotive steel, high/medium manganese steel has attracted much attention in recent years because of its attractive strength-ductility combination. Compared with the conventional process, the rapid solidification conditions in the TRC process can significantly promote the solidification structure formation, effectively inhibit element segregation, and avoid carbon loss during hot rolling.

A high manganese steel (Fe-22Mn-0.6C) strip produced by a lab-scale twin-roll caster showed a typical microstructure of dendritic and globulitic structures (Figure 14(a), (b)) [87]. The carbon content was accurate in the strip because it avoided the carbon loss that occurred during the hot rolling process. Daamen et al. [88] found that Fe-17Mn-0.6C-1.5Al as-cast strip had a fine microstructure and only slight elemental segregation on the micron scale. Since subsequent recrystallization and homogeneous annealing can eliminate segregation, there was no adverse effect on the final mechanical properties (Figure 14(c)). Besides, the grain size distribution of Fe-29Mn-0.3C strip after annealing at 900°C

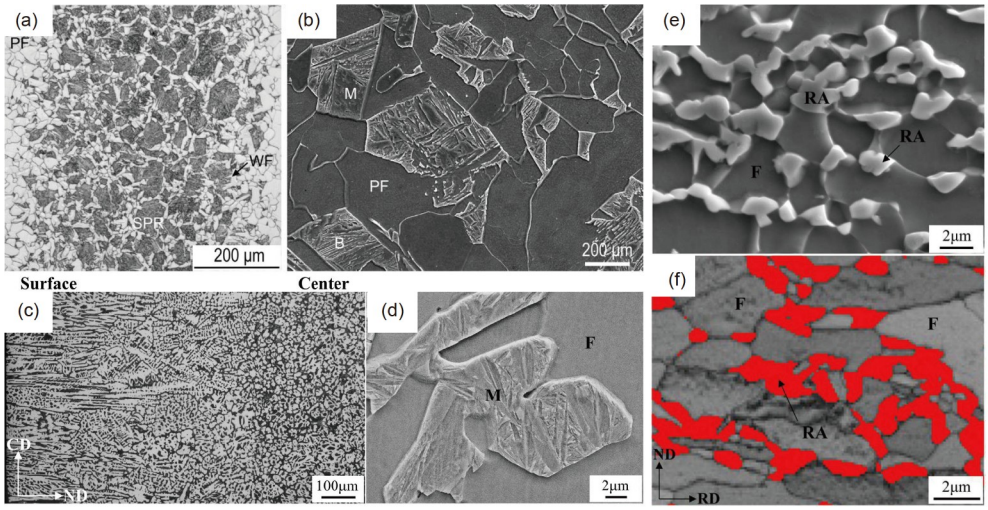

Figure 13 (Color online) TRIP steel produced by TRC. (a) Optical image of directly quenched microstructure [84]; (b) scanning electron microscope (SEM) image of directly quenched microstructure [84]; (c) optical image of the as-cast microstructure [85]; (d) SEM image of the as-cast microstructure [85]; (e) EPMA image of the final microstructure [85]; (f) EBSD image of the final microstructure [85]. (a), (b) Reprinted with permission from ref. [84] Copyright © 2016 Elsevier B.V. All rights reserved. (c)–(f) Reprinted with permission from ref. [85], Copyright © 2017 Elsevier B.V. All rights reserved.

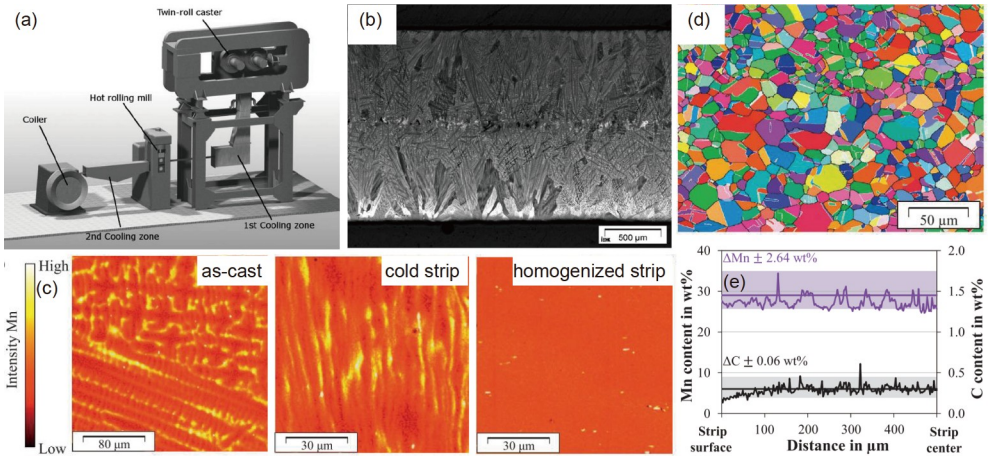

Figure 14 (Color online) TRC process of high manganese steel. (a) Lab-scale twin-roll caster [87]; (b) metallograph of the hot strip [87]; (c) element mapping of manganese content [88]; (d) EBSD mapping [89]; (e) EPMA line scan [89]. (a), (b) Reprinted with permission from ref. [87], Copyright © 2011 Wiley-VCH Verlag GmbH & Co. KGaA, Weinheim. (c) Reprinted with permission from ref. [88], Copyright © 2014 Published by Elsevier Ltd. (d), (e) Reprinted with permission from ref. [89], Copyright © 2015 Elsevier B.V. All rights reserved.

was uniform. The microsegregation was significantly reduced (Figure 14(d), (e)), and the final mechanical properties were comparable to those of advanced high-strength steel prepared by conventional process [89].

Song et al. [90] prepared a high manganese steel strip with the main component of Fe-18Mn-(0.14, 0.50)C through a TRC simulation device called injection casting (Figure 15(a)). The result demonstrated that the formation of cementite particles in the Fe-18Mn-0.50C strip was inhibited. And its mechanical properties were better than those of Fe-18Mn-0.60C steel processed by traditional hot rolling and heat-treatment. Yang et al. [91] researched various high Mn steels with the addition of Al (9 wt%) using a new TRC simulator called centrifugal casting (Figure 15(b)). They found that the 12 wt% Mn steel strip's yield strength was the highest due to the presence of dense substructure in the austenite and the TWIP effect during the deformation (Figure 16(a)–(c)). However, the comprehensive mechanical properties of 16 wt% Mn steel were the best, with tensile strength and elongation reaching 923 MPa and 46.2%, respectively.

Wang et al. [92] prepared medium manganese steel (Fe-0.3C-4Mn-1.82Al-0.6Si) using a process consisting of TRC, hot rolling, and annealing. The as-cast structure mainly presented a dendrite structure composed of martensite and

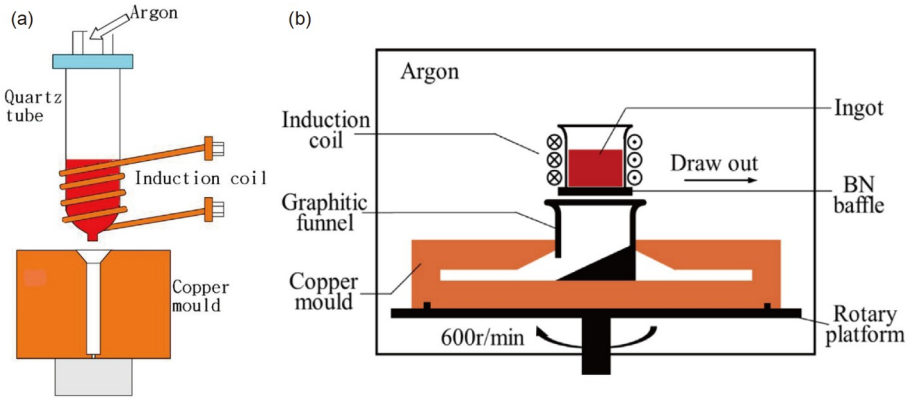

Figure 15 (Color online) TRC simulators. (a) Injecting casting equipment [90]; (b) centrifugal casting equipment [91]. (a) Reprinted with permission from ref. [90], Copyright © 2014 Elsevier B.V. All rights reserved. (b) Reprinted with permission from ref. [91], © 2019 Elsevier B.V. All rights reserved.

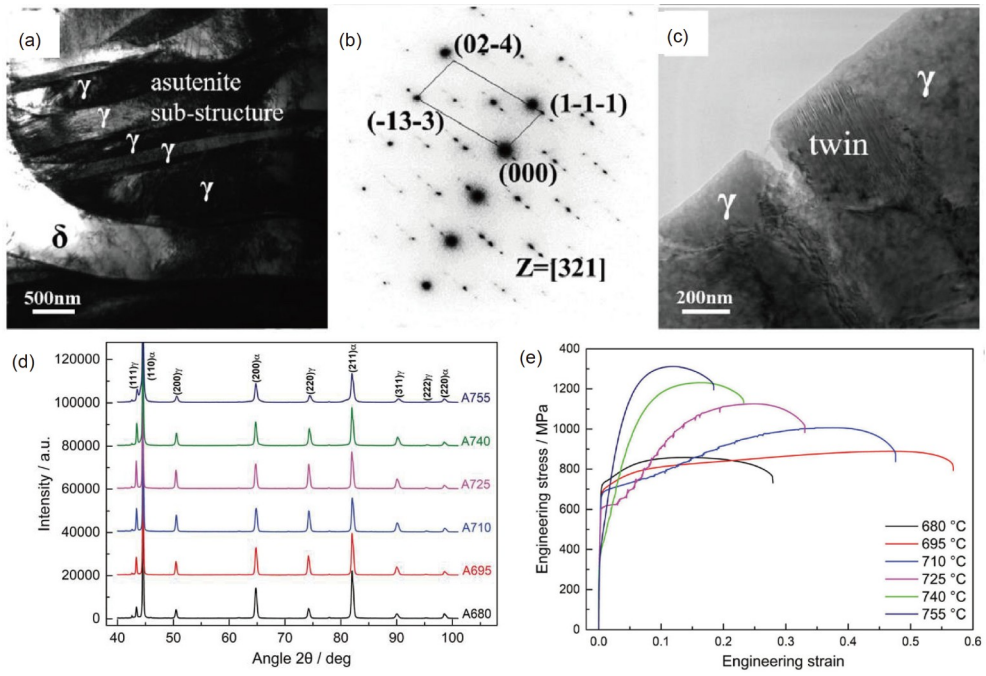

Figure 16 (Color online) Microstructure and mechanical properties of high/medium manganese steels. (a) TEM morphology of substructure in the high manganese steel [91]; (b) SAED pattern taken from the substructure area [91]; (c) twins in austenite [91]; (d) XRD patterns of the medium manganese steel [92]; (e) engineering stress-strain plots of the medium manganese steel [92]. (a)–(c) Reprinted with permission from ref. [91], © 2019 Elsevier B.V. All rights reserved. (d), (e) Reprinted with permission from ref. [92], Rights managed by Taylor & Francis.

austenite (10%). The austenite fraction was related to the annealing process. The austenite fraction after annealing at 710°C was higher (42%) with excellent mechanical properties. The tensile strength was 1007 MPa, and the elongation rate was 48% (Figure 16(d), (e)). The highest tensile strength obtained after annealing at 755°C, reached more than 1300 MPa (Figure 16(e)).

2.4.4 High strength low alloy steels

HSLA is a kind of high strength steel made by adding a small amount of alloying elements in plain carbon steel. It has the superiority characteristics of high strength, high toughness, good weldability, and corrosion resistance. The microstructure of HSLA includes acicular ferrite, bainite, and martensite, and its mechanical properties are often improved by refinement strengthening and second phase strengthening.

Most HSLA depend on the element Nb to achieve the required mechanical properties [93]. Site-specific atom probe tomography (APT) has been used to quantify Nb content in the microstructure of HSLA produced by the TRC process [94]. The result showed that Nb's content at the prior austenite grain boundary was not significantly different from that at the ferrite-ferrite grain boundary, while other elements showed significant differences (Figure 17(a), (b)). Dorin et al. [95] conducted a study on the HSLA strips produced by a dip tester. They found the coiling time and temperature had considerable effects on the yield strength due to the microstructure, which largely depended on the Nb-rich precipitates (Figure 17(c), (d)). They also studied the effect of Nb content on the transformation from austenite to bainite, and found that the Nb element can delay the bainite nucleus but accelerate the growth of bainite [96].

Moreover, the formation mechanism of MnS and Nb(C, N) in HSLA was also studied through a dip tester [97]. The result showed a higher cooling rate could significantly refine the sulfide, but Nb still exists in the matrix as a random solid solution.

Here, the mechanical properties of the above-discussed high strength steels produced by TRC are summarized in Table 4 for reference.

In conclusion, several types of high strength steels have been fabricated by the TRC process or simulators with sub-rapid solidification conditions. However, there is still a long way to improve these steels' performance and design new high-strength steels by using the TRC process.

2.5 Other types of steels

2.5.1 Copper-bearing steels

Copper is an essential residual element in scrap steel because it is difficult to remove in steelmaking [98]. Copper, which causes hot brittleness at high temperatures, is considered a harmful element in steel. Moreover, it is exceptionally urgent to recover scrap steel due to the environment's pressure and resources in recent years.

TRC process shows potential advantages in the recovery of scrap steel, because the high cooling rate can eliminate or reduce the harm of impurities and residual elements. Sellamuthu et al. [98] conducted a study on the copper-bearing steels by using the dip tester. They found copper solid-soluted in the as-cast strip but precipitated after annealing (Figure 18). The increase in copper content led to increased final product strength through solution strengthening, refinement strengthening, and precipitation strengthening [99].

Guan et al. [100] found the copper element was in a solid solution state in the copper-bearing steel with Cu concentrations below 5 wt% produced by the TRC process. But higher copper content can lead to large Cu-rich precipitates

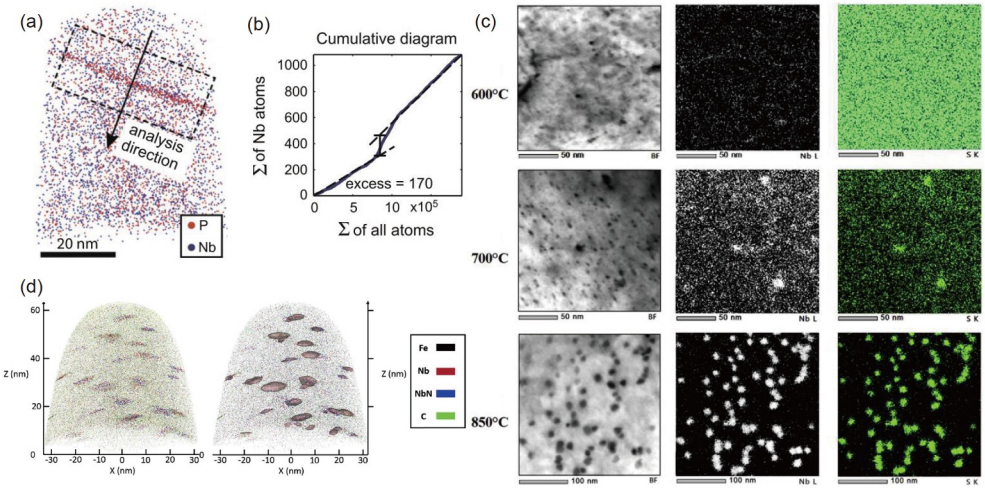

Figure 17 (Color online) Nb in the HSLA produced by TRC. (a) Atom probe technique (APT) mapping with P and Nb displayed [94]; (b) cumulative diagram taken from the APT [94]; (c) TEM images and EDS mapping of Nb-rich precipitates with different coiling temperatures [95]; (d) APT of Nb-rich precipitates with the coiling temperature of 600°C [95]. (a), (b) Reprinted with permission from ref. [94], copyright © 2012 Acta Materialia Inc. Published by Elsevier Ltd. All rights reserved. (c), (d) Reprinted with permission from ref. [95], © 2016 Acta Materialia Inc. Published by Elsevier Ltd. All rights reserved.

Table 4 Summary of mechanical properties of high strength steels produced by TRC

Type		Yield strength (MPa)	Tensile strength (MPa)	Uniform elongation (%)	Total elongation (%)	Ref.
Stainless steel	19Cr	520	1000	–	65	[42]
	2.1B	–	1182.9	–	0.9	[45]
	2.1B	–	801.1	–	14.1	[45]
DP steel	DP30	381	623	6.3	10	[78]
	DP60	290	461	17	31	[78]
	DL690	545	692	3	8	[79]
	DL650	433	621	10	21	[79]
	DT700	416	658	10	17	[80]
	DT750	386	623	14	29	[80]
	DP	350	589	–	22.4	[81]
	TC400	332	541	–	33	[81]
	HA78	621	914	–	11.03	[82]
	T600	457	518	–	29.97	[82]
TRIP steel	TQ	398	608	13	20	[83]
	T400	356	590	17	27	[83]
	TDQ	535	791	11	18	[84]
	TD400	447	696	14	26	[84]
	A78	548	945	–	28.56	[85]
	A80	515	996	–	8.89	[85]
Mn steel	29Mn	260	750	65	–	[14]
	29Mn	820	900	15	–	[14]
	17Mn	328	875	64.7	–	[88]
	17Mn	332	874	68.5	–	[88]
	29Mn	220	688	64.4	–	[89]
	29Mn	240	740	60.3	–	[89]
	12Mn	872	1056	–	17.4	[91]
	16Mn	870	974	–	47	[91]
	18Mn	300	924	–	61.3	[90]
	18Mn	290	891	–	62.0	[90]
	4Mn	–	1007	–	47.6	[92]
	4Mn	–	1320	–	18	[92]
Nb steel	0.16Nb	–	1000	–	–	[95]
Cu steel	2Cu	723	998	–	–	[98]
	5Cu	860	1076	–	–	[98]

formation, which worsens the corrosion resistance due to a mechanism that changes from pitting corrosion to selective corrosion.

2.5.2 *Sulfur-containing steels*

High strength sulfur-containing microalloyed steel is widely used in hot forgings in automotive manufacturers, such as crankshafts and connecting rods. MnS precipitates are the critical second phase precipitates in sulfur-containing steel, and they have a significant influence on the properties of steel. In particular, the reasonably distributed MnS precipitates in sulfur-containing steel can be used as an excellent lubricating medium to improve cutting performance significantly. Therefore, in the industrial production of sulfur-containing steel, it is essential to control the size/shape/distribution of MnS precipitates.

MnS precipitates in 49MnVS3 steel produced by traditional continuous casting are generally larger than 10 μm. In order to obtain products with good cutting performance, the following heat treatment process must be used to decompose MnS precipitates into less than 5 μm, which is a long time heat treatment process with high energy consumption.

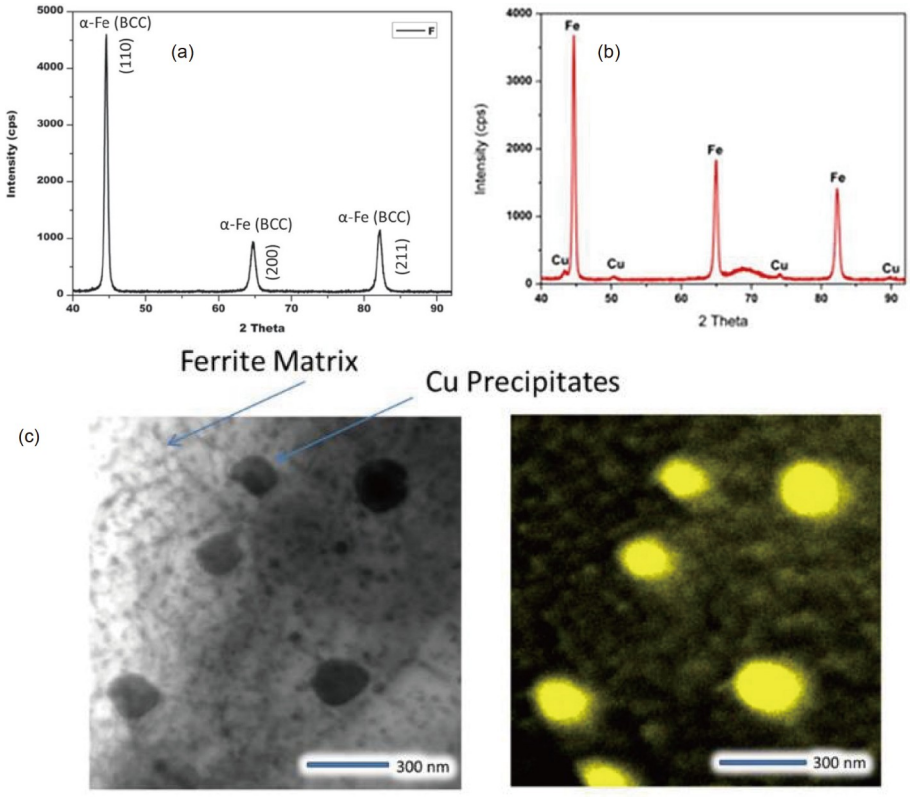

Figure 18 (Color online) Copper-bearing steel produced by dip tester for simulation of TRC [98]. (a) XRD patterns in the as-cast condition; (b) XRD patterns in the annealed condition; (c) TEM and EDS mapping of Cu precipitates.

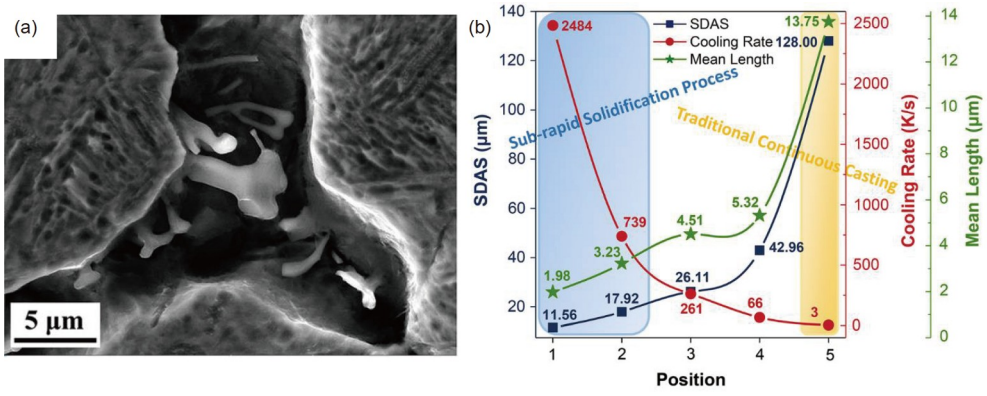

Figure 19 (Color online) Sulfur-containing steel produced by droplet solidification technique for simulation of TRC [101]. (a) SEM image of MnS precipitate; (b) relationship between the SDAS, cooling rate, and mean length of the precipitated MnS. Reprinted with permission from ref. [101], Copyright © 2019, The Minerals, Metals & Materials Society and ASM International.

Wang et al. [101] studied the precipitation behavior of MnS in sulfur-containing steel under sub-rapid solidification conditions using the droplet solidification technique. They acquired the sub-rapid solidification droplet with most MnS precipitates less than 5 μm (Figure 19(a)). And the length of MnS precipitate was found to depend linearly on the secondary dendrite arm spacing (SDAS) (Figure 19(b)), which could be precisely controlled through the cooling rate during the solidification process. The result suggested that the TRC process showed potential to produce sulfur-containing steels without an extended heat-treating process, which contributed to optimizing the traditional high energy consumption production process.

2.5.3 Clad steels

Clad steel is a representative composite material to obtain the properties that a single material does not possess. It has been widely used in many engineering applications and presents

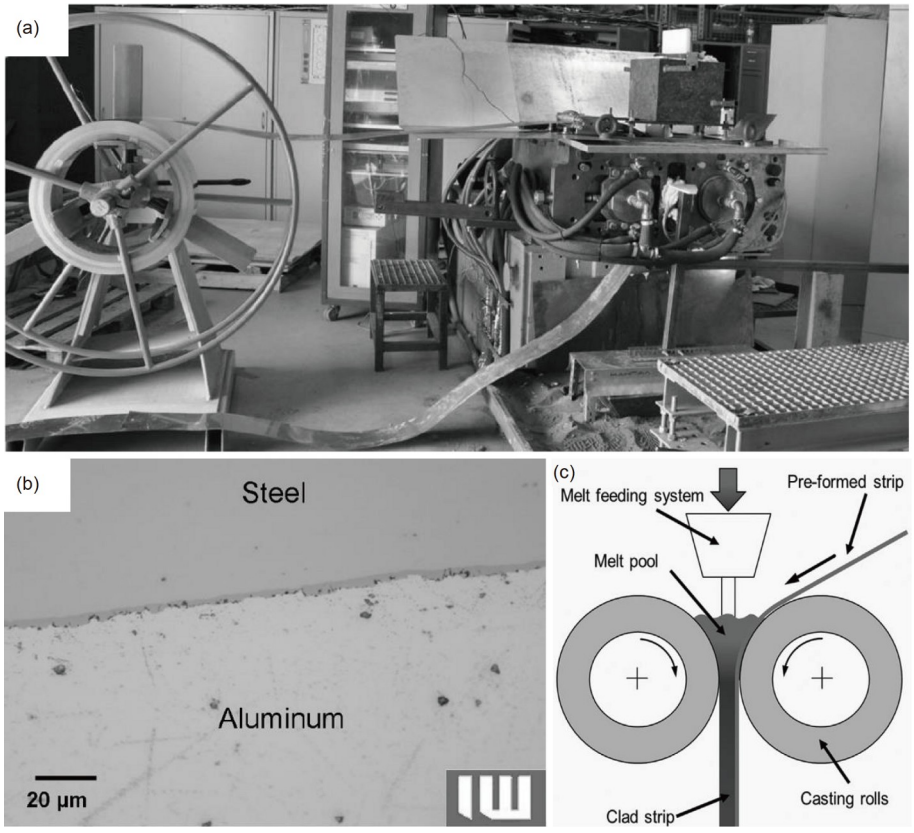

Figure 20 TRC process of clad steel strip. (a) Twin-roll strip caster for producing clad strip [102]; (b) microstructure of the seam and the parent material of the clad strip [102]; (c) schematic diagram of TRC for producing clad strip [20]. (a), (b) Reprinted with permission from ref. [102], Copyright © 2013 The Society of Manufacturing Engineers. Published by Elsevier Ltd. All rights reserved. (c) Reprinted with permission from ref. [20], © 2015 WILEY-VCH Verlag GmbH & Co. KGaA, Weinheim.

economic and performance advantages.

In principle, it is feasible to use TRC to produce clad steel. Recently, the preparation of clad steel by the TRC process is mainly in the experimental stage. At present, aluminum-steel clad strips and steel-steel clad strips have been successfully produced by the TRC process. Grydin et al. [102] made the aluminum-steel clad strips by TRC (Figure 20(a)). There were continuous, thin, and homogeneous intermetallic phases of about 3 μm thickness on the aluminum-steel interface (Figure 20(b)), and the adhesive strength was over 70 MPa. Vidoni et al. [20] produced an austenitic stainless steel-carbon steel clad strip with shear resistance at joints of 218 MPa (Figure 20(c)).

In order to improve the properties of clad steel, the hot rolling and annealing processes were used after the TRC process. The clad steel strip's bonding strength, which consists of stainless steel and high manganese steel, was increased from 250 to 400 MPa through a hot rolling process [103].

Besides, the surface roughness would influence the bonding quality of clad steel. Stolbchenko et al. [104] produced a 2.5 mm pure aluminum-austenitic stainless steel clad strip, and found that the binding strength was optimal at over 100 MPa with the surface roughness of 4.2 μm.

In a word, numerous steels, even the clad steels, have been prepared by the TRC process. So the TRC technology shows excellent applicability in the field of steel manufacturing.

3 Aluminum alloys

Lightweight engineering is one of the most promising and progressive directions of modern manufacturing [105]. With the increasing demand for automobile weight reduction, aluminum alloy shows excellent potential in replacing heavy metals such as steel. Traditional aluminum alloy production requires many processing steps, usually by casting, homogenization, scalping, cold/hot rolling, annealing, and other complex processes.

TRC technology combines casting and rolling into one step to realize sub-rapid solidification and provides an efficient and economical method for producing aluminum alloys. Although the TRC technology has been developed for several decades, only low-alloying aluminum alloys such as the 1XXX, 3XXX, 8XXX series are currently available for trial production. The increasing demand for high strength and low-cost aluminum alloys for transport has led to research into the manufacture of high alloy aluminum alloys

such as the 5XXX and 7XXX series.

Most aluminum alloys' segregation defects and surface quality problems are difficult to be removed by the heat-treatment process. These problems will lead to the final product's mechanical instability, attracting researchers' attention.

Haga et al. [106] studied the TRC process of A5182 aluminum alloy and found that the melt static pressure would enhance the heat transfer behavior between the melt and the roll, and the low superheat casting could obtain a better microstructure, in which the casting speed could be up to 150 m/min. The research of Sahoo and Ghosh [107] on Al-Cu alloys prepared by the TRC process showed that the alloy's hardness increased with the increasing of casting speed and decreased with the increasing of melt superheat. Kikuchi et al. [21] observed periodic patterns on the surface of Al-Mg alloy prepared by the TRC process and found that the oscillation of liquid metal meniscus between the surface of the roll and the nozzle tip was one of the possible reasons for the formation of periodic patterns. Wang et al. [108] reported the effect of casting parameters on the properties of 7050 aluminum alloy. They found that the alloy had the best performance when the roll gap was 1.8 mm, casting speed was 11.4 m/min, cooling water flow rate was 11.1 m^3/h, and the initial cooling water temperature was 20.8°C.

Kim et al. [109] studied the formation mechanism of central segregation in Al-Mg alloy strips. They found that with the increasing casting speed, the central segregation gradually changed from channel segregation to a segregation band (Figure 21). The deformation caused by roll separation force was the main reason for the formation of Al-Mg alloy's central segregation.

The intermetallics in the aluminum alloy are very unfavorable for tensile properties because of their brittleness and stress concentration. The work of Liu et al. [110] on AA5083 strips with different Fe, Si content showed that the size and density of intermetallic particles increased with Fe, Si content. Song et al. [111] found that there were fine second phase particles in the Al-Mn-Fe alloy strips, while the solute distribution in the Al-Mn-Si alloy was relatively uniform, which was due to the higher cooling rate in the TRC process.

Melt conditioning technology uses a high shear force agitator to regulate liquid metal before casting. The alloy AA6111 [112] and AA5754 [113] produced by TRC with melt conditioning technology showed that less centerline segregation and fine equiaxial crystal structure, and the cast strip quality was significantly improved, which was superior to the cast strip without melt conditioning technology (Figure 22). Furthermore, the mechanical test showed that the hardness of the alloy was improved significantly after applying melt conditioning and thermo-mechanical treatment.

He et al. [114] conducted exciting research on the effect of outfields (electric and magnetic fields) on the AA6022 alloy and found that the application of outfields not only improved the uniformity of microstructure and chemical composition but also increased the strength and elongation of the alloy (Figure 23).

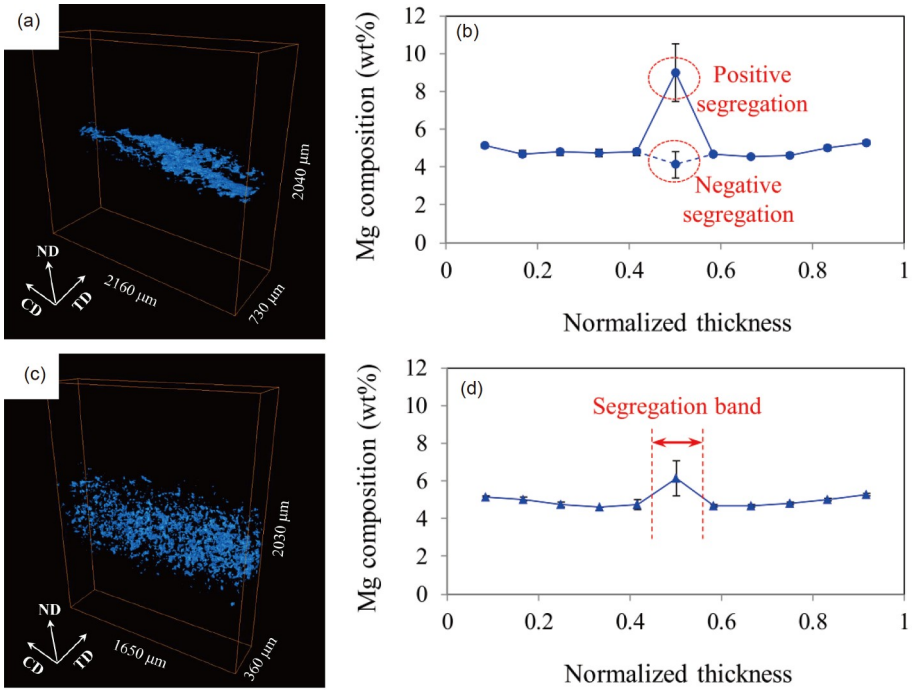

Figure 21 (Color online) Segregation of Al-Mg strip produced by TRC [109]. 3D images of the center segregation in strip manufactured at (a) 3 m/min, and (b) 5 m/min. Mg composition along the thickness direction in strip manufactured at (c) 3 m/min, and (d) 5 m/min. Reprinted with permission from ref. [109], © 2018 Acta Materialia Inc. Published by Elsevier Ltd. All rights reserved.

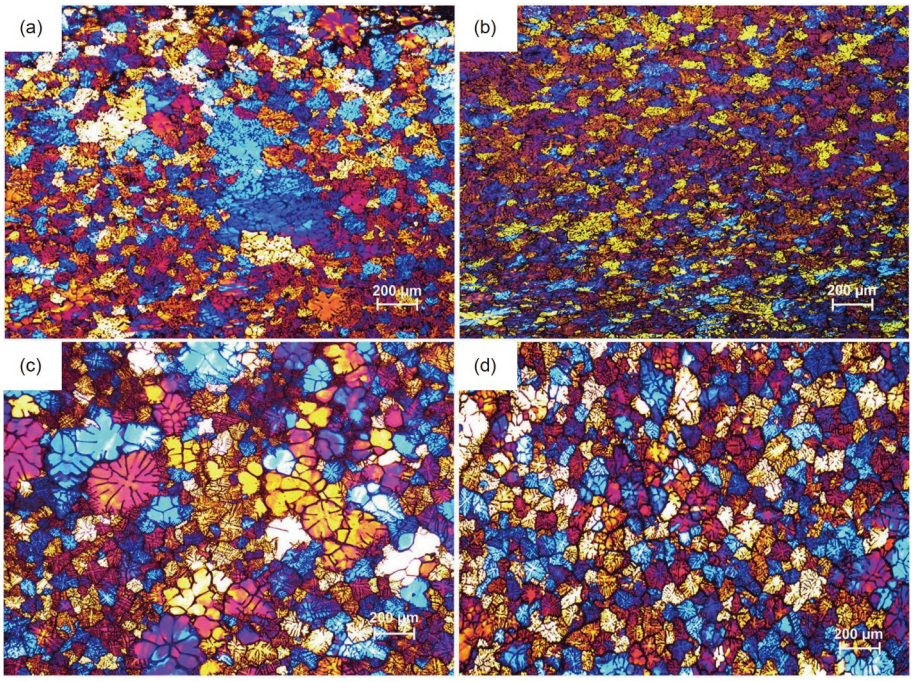

Figure 22 (Color online) Optical micrographs of as-cast AA6111 [112]. Normal direction of as-cast AA6111 produced (a) by conventional TRC, and (b) by Melt-conditioned TRC. Transverse section of as-cast AA6111 produced (c) by conventional TRC, and (d) by Melt-conditioned TRC.

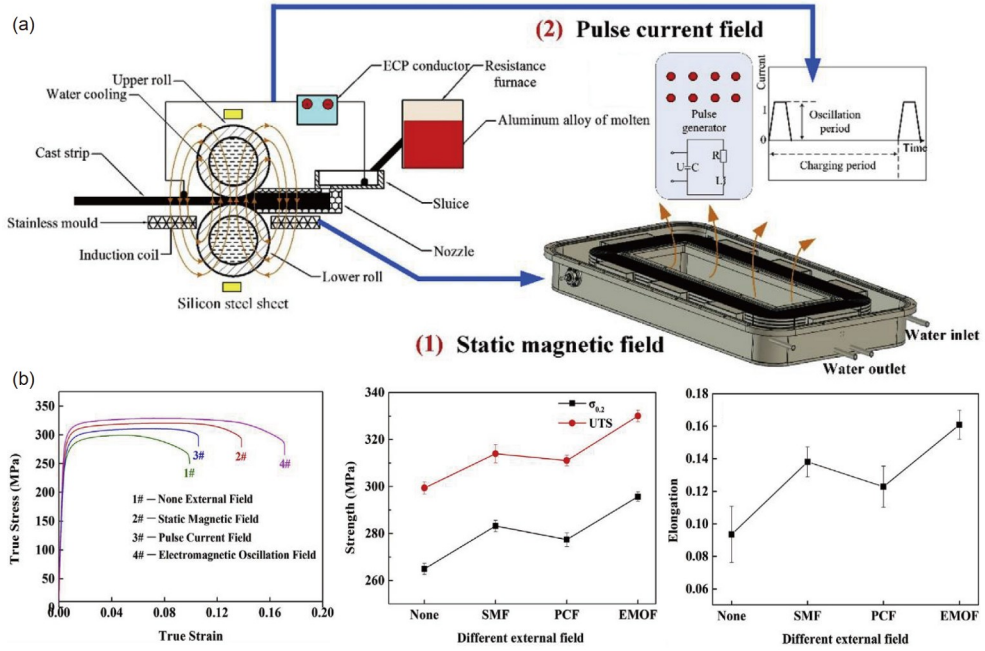

Figure 23 (Color online) External field aided TRC [114]. (a) Schematic of the TRC process with different external fields; (b) mechanical properties of the cast-rolled strips with different external fields. Reprinted with permission from ref. [114], © 2019 Elsevier B.V. All rights reserved.

4 Magnesium alloys

With the increasing demand for light vehicle structure, magnesium alloy is a suitable candidate material to replace steel and aluminum in the automotive industry, and has been used in the automotive, aerospace, national defense, and electronics industries [115]. More importantly, magnesium alloy has good biocompatibility and mechanical properties that have the potential to be widely used in medical biomaterials [116]. Whereas until now, only a few studies have been conducted on the TRC process of magnesium alloys [117].

It is worth mentioning that two novel techniques aided in the TRC process of magnesium alloys. Melt-conditioned TRC, which has been discussed before, was also applicable

to magnesium alloy strips' production. The AZ31 Mg alloy strips were produced by melt-conditioned TRC, and the alloy's mechanical properties were improved by the refined and uniform microstructure, reduced centerline segregation, and smaller deformation [118].

The mechanical properties of metallic materials can be significantly affected by improving the solidification behavior of metallic materials with high-intensity ultrasound [119]. A High-intensity ultrasound-assisted TRC process has been used to prepare magnesium alloy to improve its properties, and the result showed that ultrasonic treatment improved the strength, elongation, and ultimate drawing ratio of the alloy [120]. Refinement of α-Mg grains and modification of $Mg_{17}(Al, Zn)_{12}$ and AlCeMn phases in the microstructure were the main reasons for improving the properties.

5 Metallic glasses

Metallic glasses (MGs) are usually obtained by direct quenching molten metallic matrix to avoid crystallization, and the long-range disordered structure makes MGs possess unique mechanical and physical properties, such as high strength, high hardness, high elastic limit, low elastic modulus, good corrosion resistance and excellent soft magnetic properties [121]. As a new potential structural material, MG has attracted much attention because of its superb processing performance under supercooling.

However, the traditional single-roll melt spinning method can only produce thin amorphous strips with a thickness of no more than 150 μm (Figure 24(a)); and manufacturing thicker amorphous strips remains challenging [122]. In order to overcome this limitation, TRC technology has been used in the pilot production of the amorphous strips, such as Ti-base, Mg-base, Zr-base, and ZrCu-base MGs in recent years. Seki et al. [123] studied the amorphous $Ti_{47.4}Cu_{42}Zr_{5.3}TM_{5.3}$ (TM = Co, Fe) and found that the strip had a flat surface with a strong white luster and showed apparent vitrification transformation, mainly in the glass phase. Also, the amorphous strip had good flexural ductility, and its Vickers hardness was up to 590–600.

The $Mg_{60}Cu_{29}Gd_{11}$ MG strips with thicknesses between 1 and 4 mm were produced by East et al. [124]. The result showed that the maximum bending stress was 150 MPa, bending strain was 0.005, and Charpy impact energy was 0.02 J.

The $Zr_{41.2}Ti_{13.8}Cu_{12.5}Ni_{10}Be_{22.5}$ strips with a thickness of 320 and 490 μm were prepared by Zhang et al. [122] (Figure 24(b)–(d)). They found that the increase in the thickness of the thin band resulted in a lower energy state, lower enthalpy of relaxation, lower content of free volume, and higher hardness. Lee and Lee [125] produced the $Cu_{36}Zr_{48}Al_8Ag_8$ amorphous strip with a length of more than 250 mm, and Al-rich and Ag-depleted crystalline phases crystal phase was confirmed in the microstructure (Figure 24(e)). The good plasticity of amorphous alloys in the tensile deformation mode was due to the presence of a small amount of dendritic crystalline phase in the amorphous matrix.

Wu et al. designed a new triple twin-roller casting device to produce MG strips (Figure 25(a)) [18], which created a faster cooling rate through the unique triple layer design, and could effectively avoid crystallization. It is a suitable technology for producing thin amorphous strips.

Using the novel TRC device, two prepared MG strips ($Zr_{41.2}Ti_{13.8}Cu_{12.5}Ni_{10}Be_{22.5}$ and $Zr_{55}Cu_{30}Al_{10}Ni_5$) were obtained in the fully amorphous state (Figure 25(b)–(e)), and they showed an excellent elastic energy storage capacity under a three-point bending test.

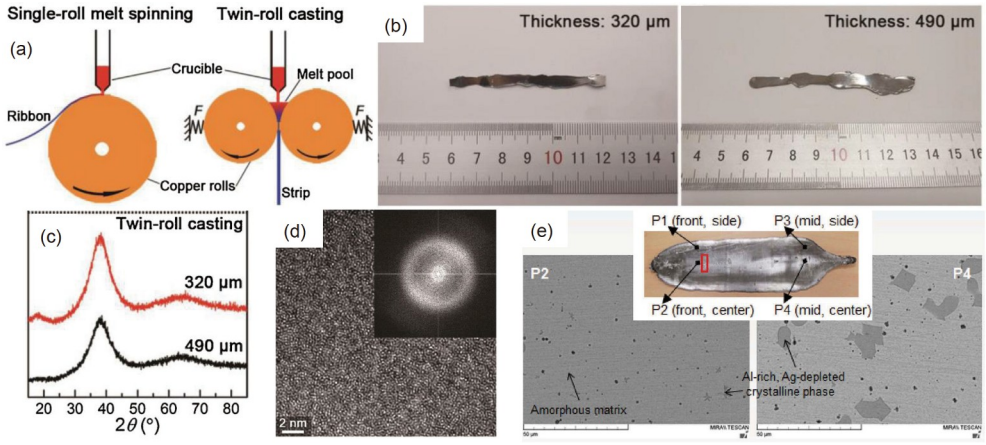

Figure 24 (Color online) TRC process of MGs. (a) Schematic illustration of single-roll melting spinning and TRC for producing MGs [122]; (b) strips prepared by TRC [122]; (c) XRD spectra of the strips [122]; (d) HRTEM image with an inset of the FFT pattern of the strip [122]; (e) SEM image of the Al-rich and Ag-depleted crystalline phases [125]. (a)–(d) Reprinted with permission from ref. [122], Copyright © 2020, Elsevier. (e) Reprinted with permission from ref. [125], Rights managed by Taylor & Francis.

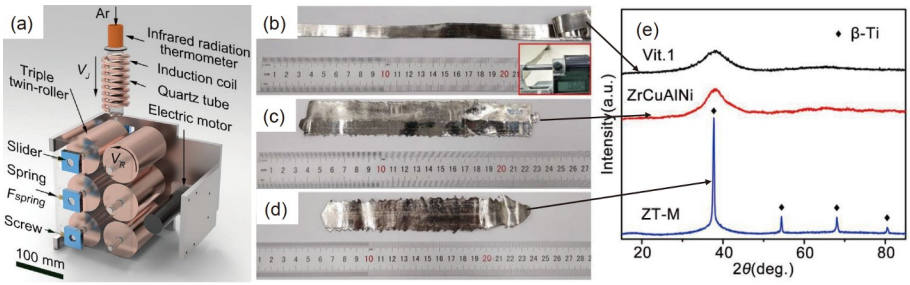

Figure 25 (Color online) MGs produced by a novel TRC [17]. (a) 3D model of the triple TRC device; (b) $Zr_{41.2}Ti_{13.8}Cu_{12.5}Ni_{10}Be_{22.5}$ strip; (c) $Zr_{55}Cu_{30}Al_{10}Ni_5$ strip; (d) MG composite strip; (e) XRD spectra of the strips.

6 Other alloys and composites

6.1 TiAl alloy

TiAl-based alloys are widely used in the field of high-temperature structural parts such as turbines, hollow blades, aero-engine exhaust nozzles, and honeycomb structures, due to their low density, high-temperature strength, and high creep resistance. However, TiAl alloy shows low ductility and poor formability, making it difficult to produce high-quality products by a conventional process.

In contrast, the TRC process is suitable for the preparation of TiAl alloy, which could overcome the above difficulty. The crack-free Ti-43Al alloy strip with 1000 mm×110 mm×2 mm was prepared by the TRC process [126]. Its microstructure was columnar grain growing externally and equiaxed grain at the center, and there was severe element segregation along the thickness direction. Furthermore, the heat treatment process was used to improve the homogeneity of microstructure; finally, multiple microstructures of near gamma, near-layer, and full-layer were obtained.

6.2 Inconel 718 alloy

Inconel 718 (IN718), as the most widely used high-temperature alloy, has been successfully applied to critical high-temperature structures such as gas turbine disc, rocket/aircraft engine, and a nuclear reactor, due to its sufficient strength, high ductility, and good fatigue resistance above 650°C. Nb-rich precipitates (mainly Laves phase) are the most common brittle precipitates formed in the superalloys. Therefore, appropriate regulatory measures must be taken to eliminate or refine Nb-rich precipitates to reduce the harm. In industry, as-cast superalloys are usually heat treated for a long time to dissolve Nb-rich precipitates in the matrix, but this treatment method has high energy consumption.

For the TRC process simulation, a droplet solidification technique was used to prepare the sub-rapid solidified IN718 alloy [127]. The result showed that the TRC process was an essential method to improve the quality of superalloy by adjusting the microstructure, refining grain, and reducing the size of Nb-rich precipitates (Figure 26).

6.3 Al-matrix composites

Al-matrix composites are attractive and viable candidates for many militaries, aerospace, and automobile applications, due to their lightweight and high performance [128]. Fiber-reinforced Al-matrix composites have excellent properties such as lightweight, high specific strength, specific modulus, wear resistance, heat resistance, thermal conductivity, etc., and have broad application prospects for automotive, aerospace, and advanced weapons industries.

TRC was used to prepare the Al-matrix composite using a 304 stainless steel wire mesh with an Al 1060 matrix. This TRC process is called a solid-liquid cast-roll bonding process (Figure 27(a)) [129]. No macroscopic defects were found at the bonding interface (Figure 27(b)). Besides, the tensile test result showed that the tensile strength and elon-

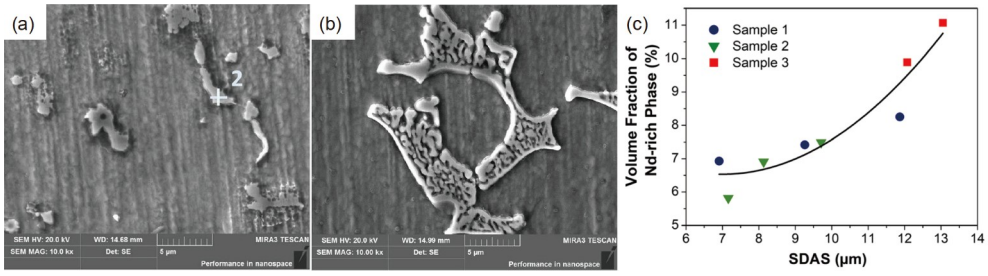

Figure 26 (Color online) IN718 produced by TRC [127]. (a) Nb-rich precipitates with sub-rapid cooling; (b) Nb-rich precipitates with air cooling; (c) relationship between the SDAS and volume fraction of Nb-rich precipitates. Reprinted with permission from ref. [127], Copyright © 2020, The Minerals, Metals & Materials Society and ASM International.

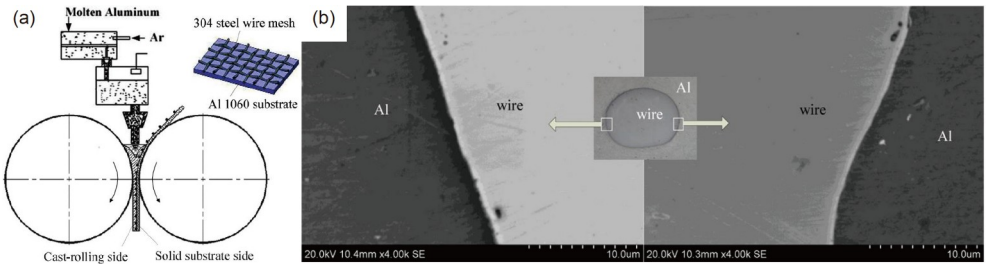

Figure 27 (Color online) Al-matrix composite plate produced by TRC [129]. (a) Schematic diagram of the TRC process; (b) SEM image of the local bonding interface.

gation of the composite plate could be increased by increasing the steel wire's orientation angle relative to the rolling direction. When the directional angle was 45°, the tensile strength and elongation reached the maximum.

7 Summary and outlook

7.1 Summary

In this review, we have briefly introduced the concept of TRC technology and its advantages first. Then, we made extensive discussions on state of the art in TRC process in the field of preparation of advanced metallic materials, including plain carbon steels, stainless steels, Fe-Si electrical steels, high-strength steels, clad steels, aluminum alloys, magnesium alloys, metallic glasses, and other alloys or composites. These results showed the remarkable universality of TRC in the area of materials fabrication.

It is important to mention that TRC is a crucial method to tackle elements segregation, inclusions precipitation, nonuniform solidification, and microstructure coarsening, etc., in the processing of metallic materials. For example, MnS precipitates' sizes in high-sulfur microalloyed steel (49MnVS3) produced by the sub-rapid solidification process are much less than that of the conventional continuous casting. Also, TRC has shown considerable superiority for controlling element segregation and secondary phase precipitation behaviors in the processing of stainless steel, manganese steel, and other types of steel. Besides, TRC is an essential method to improve the quality of superalloy by adjusting the microstructure, refining grain, and reducing the size of Nb-rich precipitates.

7.2 Outlook

It is generally known that steels showing a variety of excellent performances, are still the most widely used raw metal materials with the broadest application range. In order to explore the ultimate performance and develop novel metallurgical processing for green manufacturing of advanced steel materials with cost reduction and energy saving; consequently, an outlook on future opportunities in the TRC process of two special steels are provided.

7.2.1 Fe-Si electrical steels

As discussed in Section 2, several types of steels have been successfully produced by the TRC process. Fe-Si electrical steels are the most successful types among them. TRC process has fabricated both NOES and GOES with different Si content from 0.7 to 6.5 wt%. Tables 2 and 3 are shown the magnetic properties of the TRC processed electrical steels. The highest magnetic induction and lowest iron loss of NOES with 0.7–3.2 wt% Si produced by TRC were 1.806 (B_{50}) and 2.92 ($P_{15/50}$), and they were 1.98 (B_8) and 0.7 ($P_{17/50}$) for the cases of GOES with 2.8–4.5 wt% Si. Besides, the highest magnetic induction and lowest iron loss of high Si NOES with 6.5 wt% Si were 1.59 (B_{50}) and 0.645 ($P_{10/50}$).

These results confirmed the TRC process has already been adapted for the manufacturing of high-performance electrical steels. Meanwhile, most of the strips produced by the actual caster or pilot caster with standard thicknesses of 0.5, 0.35, 0.23, and 0.2 mm, could easily meet the industrial requirement of commercial strips. For this reason, we are confident that a variety of electrical steels would eventually be produced by industrial TRC process, and could be widely used in the varieties of fields.

7.2.2 Ultrahigh strength steels

The exploration of the ultimate mechanical property of high strength steels has never stopped. Ultrahigh strength steels (UHSSs) typically have a tensile strength of over 1500 MPa, and they are used in the most challenging structural applications, such as high-performance shafts, high strength fasteners, aircraft landing gear, rocket housings, etc [130]. UHSSs have been developed for decades and include the following categories: low alloyed ultrahigh strength steels, maraging steels, secondary hardening steels, precipitation hardening stainless steels, etc.

In recent years, to overcome a dilemma known as strength-ductility trade-off, nanobainitic steels [131], deformed and partitioned steels [132], high-density nanoprecipitation steels [133], low-density steels [3], and others were developed as the new promising types of UHSSs. Their mechanical

properties are characterized by an excellent combination of strength and ductility or toughness.

For example, an ultra-strong 8Mn steel (strength levels beyond 2.0 GPa) with good ductility (20%) (Figure 28) [134], and an ultra-strong 10Mn steel with a yield strength of 2.0 GPa and fracture toughness of 102 MPa m½ has been developed recently [135]. Also, low alloy high carbon martensitic steel with a strength of 2.6 GPa and elongation of 7% was obtained [136]. These meaningful works highlight the importance of exploring the ultimate performance of UHSSs.

TRC process with sub-rapid solidification characteristics has remarkable potential for reducing segregation and large participates, refining microstructure, and further improving materials' properties. It should be an appropriate way to produce UHSSs. But from Table 4, it can be concluded the tensile strengths of the majority high strength steels produced by TRC were no more than 1000 MPa. It ought to be noted that most previous studies were only conducted on traditional high strength steels, not the UHSSs; not surprisingly, the obtained mechanical properties were far from the level of UHSSs. Therefore, it is imperative to conduct more research on the TRC process of UHSSs.

The martensite structure, ultrafine grain, and elements segregation are three typical technical issues that should be considered for developing the TRC process of UHSSs. Martensite is the main structure in UHSSs, and it is usually acquired under a rapid cooling rate, which could be easily achieved in the process of TRC. Therefore, TRC may be suitable for producing maraging steels, press hardening steels (PHS), quenching and partitioning (Q&P) steels, medium manganese steels, or other steels that need a rapid cooling rate to obtain the martensite structure.

Refinement strengthening is a vital manner to improve the strength without reduction of ductile and toughness, and it has successfully achieved in the case of micro-alloy steels by using the deformation induced ferrite transformation, which results in the increasement of yield strength from 400 to 800 MPa with refined grains to the micron level [137]. Microstructure refinement usually occurs during the TRC process because of the sub-rapid solidification and the followed fast cooling. So, TRC would be easier to achieve refined grains than the conventional process. As a result, it is urgent to conduct such research by taking advantage of TRC process.

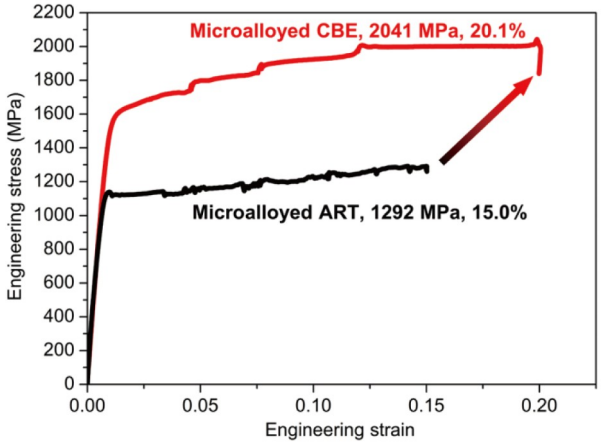

Figure 28 (Color online) Mechanical properties of ultrastrong steels [134].

Alloying elements are prone to segregate during the conventional casting process of maraging steels, secondary hardening steels, or other high alloyed steels. This phenomenon resulted in composition inhomogeneity and would lead to cracking in engineering applications. Prolonging the heat treatment time to homogenize the composition would dramatically increase energy consumption and production efficiency. TRC process with a rapid cooling rate during solidification can reduce segregation substantially. Thus, it might be suitable for the processing of high alloyed UHSSs.

In addition, the research and development of UHSSs should coordinately consider the composition design, principle of microstructure control, industrial production, evaluation of service performance, etc. The transition from the single microstructure control to the cooperative management of complex multiphase, multiscale structure, chemical boundary, and inhomogeneity, would require a combination of various metallurgical processing.

The recently developed new types of UHSSs, for example, the deformed and partitioned steels, combine several complicated metallurgical processes to gain the required microstructure and outstanding performance. Hence, it is too harsh for the TRC process to replace the conventional process thoroughly; by contrast, it should be served as a promising technology to replenish and upgrade the specific stage of the conventional process of UHSSs.

7.2.3 Green manufacturing

Our goal is to achieve green manufacturing technology for advanced steels through near-net-shape processing technology. TRC can provide a variety of advantages for the production of advanced steels, i.e., the non-equilibrium solidification, supersaturated solid solution of alloying elements, and unique homogenized structure during the process, which would offer a feasible technical means for the preparation of industrial-scale wide-width homogeneous strip with low cost and consume.

However, despite such technological advantages, there still exist considerable challenges to be tackled, i.e., liquid level fluctuation control, control of interfacial cooling, sub-rapid solidification and its related structure, second phase precipitation, etc. It should be implemented by combining solidification, solid-state transformation, and deformation; simultaneously, the controlling of structure and properties need to be integrated. Finally, the improvement of quality and performance of steel products could be realized. There is

still a long way to industrialize the manufacture of advanced metallic materials through the TRC process. Yet all the efforts would be worth for sustainable development of materials' society.

This work was supported by the National Natural Science Foundation of China (Grant Nos. U1760202, 51904345), Hunan Provincial Key Research and Development Program (Grant No. 2018WK2051), and the State Scholarship Fund from the China Scholarship Council (Grant No. 201906370153).

1 Plummer J. Metallurgy is key. Nat Mater, 2016, 15: 699–700
2 Raabe D, Tasan C C, Olivetti E A. Strategies for improving the sustainability of structural metals. Nature, 2019, 575: 64–74
3 Kim S H, Kim H, Kim N J. Brittle intermetallic compound makes ultrastrong low-density steel with large ductility. Nature, 2015, 518: 77–79
4 Nolli P. Initial solidification phenomena: Factors affecting heat transfer in strip casting. Dissertation for Doctoral Degree. Pittsburgh: Carnegie Mellon University, 2007
5 Zhu C, Wang W, Lu C. Sub-rapid solidification and its related interfacial heat-transfer behaviors in strip casting process. J Sust Metall, 2019, 5: 378–390
6 Campbell P, Blejde W, Mahapatra R, et al. Recent progress on commercialization of castrip® direct strip casting technology at Nucor Crawfordsville. Metallurgist, 2004, 48: 507–514
7 Dai Y, Xu Z, Luo Z, et al. Phase formation kinetics, hardness and magnetocaloric effect of sub-rapidly solidified $LaFe_{11.6}Si_{1.4}$ plates during isothermal annealing. J Magn Magn Mater, 2018, 454: 356–361
8 Girgensohn A, Büchner A R. Twin roll strip casting of low carbon steels. Ironmak Steelmak, 2013, 27: 317–323
9 Ge S, Isac M, Guthrie R I L. Progress of strip casting technology for steel: Historical developments. ISIJ Int, 2012, 52: 2109–2122
10 Park J Y, Oh K H, Ra H Y. Texture and deformation behaviour through thickness direction in strip-cast 4.5wt% Si steel sheet. ISIJ Int, 2000, 40: 1210–1215
11 Yamamoto K, Matsuura M, Sugimoto S. Microstructure formation in strip-cast RE-Fe-B alloys for magnets. Metall Mat Trans A, 2017, 48: 3482–3489
12 Mizoguchi T, Miyazawa K. Formation of solidification structure in twin roll casting process of 18Cr-8Ni stainless steel. ISIJ Int, 1995, 35: 771–777
13 Chen H, Xu W, Tang C, et al. Intragranular glass/crystal conjugated particles in strip cast Nd-Fe-B flakes. J Magn Magn Mater, 2020, 495: 165863
14 Daamen M, Güvenç O, Bambach M, et al. Development of efficient production routes based on strip casting for advanced high strength steels for crash-relevant parts. CIRP Ann, 2014, 63: 265–268
15 Zhang W, Yu Y, Fang Y, et al. Determination of interfacial heat flux of stainless steel solidification on copper substrate during the first 0.2 s. J Shanghai Jiaotong Univ (Sci), 2011, 16: 65–70
16 Dou W X, Yuan G, Lan M F, et al. The significance of microstructure and texture on magnetic properties of non-oriented silicon steel: Strip casting versus conventional process. Steel Res Int, 2020, 91: 1900286
17 Wang W, Zhu C, Lu C, et al. Study of the heat transfer behavior and naturally deposited films in strip casting by using droplet solidification technique. Metall Mat Trans A, 2018, 49: 5524–5534
18 Wu Y, Zhang L, Chen S, et al. A multiple twin-roller casting technique for producing metallic glass and metallic glass composite strips. Materials, 2019, 12: 3842
19 Guo J, Liu Y, Liu L, et al. 3D stress simulation and parameter design during twin-roll casting of 304 stainless steel based on the Anand model. Int J Miner Metall Mater, 2014, 21: 666–673
20 Vidoni M, Ackermann R, Richter S, et al. Production of clad steel strips by twin-roll strip casting. Adv Eng Mater, 2015, 17: 1588–1597
21 Kikuchi D, Harada Y, Kumai S. Surface quality and microstructure of Al-Mg alloy strips fabricated by vertical-type high-speed twin-roll casting. J Manuf Process, 2019, 37: 332–338
22 Chen M, Hu X D, Han B, et al. Study on the microstructural evolution of AZ31 magnesium alloy in a vertical twin-roll casting process. Appl Phys A, 2016, 122: 91
23 Zapuskalov N. Comparison of continuous strip casting with conventional technology. ISIJ Int, 2003, 43: 1115–1127
24 Ge S, Isac M, Guthrie R I L. Progress in strip casting technologies for steel: Technical developments. ISIJ Int, 2013, 53: 729–742
25 Maleki A, Taherizadeh A, Hosseini N. Twin roll casting of steels: An overview. ISIJ Int, 2017, 57: 1–14
26 Zhao J, Jiang Z. Thermomechanical processing of advanced high strength steels. Prog Mater Sci, 2018, 94: 174–242
27 Dong H. Year 2020: 200th anniversary for alloy steel-preword of special issue for alloy steel (in Chinese). Acta Metall Sin, 2020, 56: 1-IV
28 Guillet A, Es-Sadiqi E, L'EspÉRance G, et al. Microstructure and mechanical properties of strip cast 1008 steel after simulated coiling, cold rolling and batch annealing. ISIJ Int, 1996, 36: 1190–1198
29 Tavares R P, Isac M, Guthrie R I L. Roll-strip interfacial heat fluxes in twin-roll casting of low-carbon steels and their effects on strip microstructure. ISIJ Int, 1998, 38: 1353–1361
30 Laleh M, Hughes A E, Xu W, et al. Unexpected erosion-corrosion behaviour of 316L stainless steel produced by selective laser melting. Corrosion Sci, 2019, 155: 67–74
31 Wang Y M, Voisin T, McKeown J T, et al. Additively manufactured hierarchical stainless steels with high strength and ductility. Nat Mater, 2018, 17: 63–71
32 Yasunaka H, Taniguchi K, Kokita M, et al. Surface quality of stainless steel type 304 cast by twin-roll type strip caster. ISIJ Int, 1995, 35: 784–789
33 Choo D K, Moon H K, Kang T, et al. Analysis and prevention of cracking during strip casting of AISI 304 stainless steel. Metall Mat Trans A, 2001, 32: 2249–2258
34 Ha M, Choi J, Jeong S, et al. Analysis and prevention of microcracking phenomenon occurring during strip casting of an AISI 304 stainless steel. Metall Mat Trans A, 2002, 33: 1487–1497
35 Hunter A, Ferry M. Texture enhancement by inoculation during casting of ferritic stainless steel strip. Metall Mat Trans A, 2002, 33: 1499–1507
36 Hunter A, Ferry M. Evolution of microstructure and texture during casting of AISI 304 stainless steel strip. Metall Mat Trans A, 2002, 33: 3747–3754
37 Liu H T, Liu Z Y, Qiu Y Q, et al. Characterization of the solidification structure and texture development of ferritic stainless steel produced by twin-roll strip casting. Mater Charact, 2009, 60: 79–82
38 Strezov L, Herbertson J. Experimental studies of interfacial heat transfer and initial solidification pertinent to strip casting.. ISIJ Int, 1998, 38: 959–966
39 Spinelli J E, Tosetti J P, Santos C A, et al. Microstructure and solidification thermal parameters in thin strip continuous casting of a stainless steel. J Mater Processing Tech, 2004, 150: 255–262
40 Strezov L, Herbertson J, Belton G R. Mechanisms of initial melt/substrate heat transfer pertinent to strip casting. Metall Materi Trans B, 2000, 31: 1023–1030
41 Zhu C, Wang W, Zeng J, et al. Interactive relationship between the superheat, interfacial heat transfer, deposited film and microstructure in strip casting of duplex stainless steel. ISIJ Int, 2019, 59: 880–888
42 Zhao Y, Zhang W, Liu X, et al. Development of TRIP-aided lean duplex stainless steel by twin-roll strip casting and its deformation mechanism. Metall Mat Trans A, 2016, 47: 6292–6303
43 Hao Y, Cao G, Li C, et al. The aging precipitation behavior of 20Cr-24Ni-6Mo super-austenitic stainless steel processed by conventional

casting and twin-roll strip casting. Mater Charact, 2019, 147: 21–30
44 Hao Y, Cao G, Li C, et al. Solidification structures of Fe-Cr-Ni-Mo-N super-austenitic stainless steel processed by twin-roll strip casting and ingot casting and their segregation evolution behaviors. ISIJ Int, 2018, 58: 1801–1810
45 Wang Z J, Huang X M, Li Y W, et al. Ultra-fine microstructure and excellent mechanical properties of high borated stainless steel sheet produced by twin-roll strip casting. Mater Sci Eng-A, 2019, 747: 185–196
46 Sha Y H, Sun C, Zhang F, et al. Strong cube recrystallization texture in silicon steel by twin-roll casting process. Acta Mater, 2014, 76: 106–117
47 Li H Z, Liu H T, Liu Z Y, et al. Microstructure, texture evolution and magnetic properties of strip-casting non-oriented 6.5 wt.% Si electrical steel doped with cerium. Mater Charact, 2015, 103: 101–106
48 Li H Z, Liu H T, Liu Z Y, et al. Characterization of microstructure, texture and magnetic properties in twin-roll casting high silicon non-oriented electrical steel. Mater Charact, 2014, 88: 1–6
49 Li H Z, Liu H T, Liu Y, et al. Effects of warm temper rolling on microstructure, texture and magnetic properties of strip-casting 6.5 wt% Si electrical steel. J Magn Magn Mater, 2014, 370: 6–12
50 Xu Y, Jiao H, Qiu W, et al. Effect of cold rolling process on microstructure, texture and properties of strip cast Fe-2.6%Si steel. Materials, 2018, 11: 1161
51 Li H Z, Wang X L, Liu H T, et al. Microstructure, texture evolution, and magnetic properties of strip-casting nonoriented 6.5 wt.% Si electrical steel sheets with different thickness. IEEE Trans Magn, 2015, 51: 1–4
52 Xu Y B, Zhang Y X, Wang Y, et al. Evolution of cube texture in strip-cast non-oriented silicon steels. Scripta Mater, 2014, 87: 17–20
53 Liu H T, Li H Z, Li H L, et al. Effects of rolling temperature on microstructure, texture, formability and magnetic properties in strip casting Fe-6.5 wt% Si non-oriented electrical steel. J Magn Magn Mater, 2015, 391: 65–74
54 Chen A, Li H. Microstructure and texture of 0.75%Si non-oriented electrical steel fabricated by strip casting process. Metallogr Microstruct Anal, 2016, 5: 428–434
55 Liu H T, Wang Y P, An L Z, et al. Effects of hot rolled microstructure after twin-roll casting on microstructure, texture and magnetic properties of low silicon non-oriented electrical steel. J Magn Magn Mater, 2016, 420: 192–203
56 Jiao H, Xu Y, Xu H, et al. Influence of hot deformation on texture and magnetic properties of strip cast non-oriented electrical steel. J Magn Magn Mater, 2018, 462: 205–215
57 Xu Y, Jiao H, Zhang Y, et al. Effect of pre-annealing prior to cold rolling on the precipitation, microstructure and magnetic properties of strip-cast non-oriented electrical steels. J Mater Sci Tech, 2017, 33: 1465–1474
58 Wang Y Q, Zhang X M, Zu G Q, et al. Effect of hot band annealing on microstructure, texture and magnetic properties of non-oriented electrical steel processed by twin-roll strip casting. J Magn Magn Mater, 2018, 460: 41–53
59 Fang F, Xu Y B, Zhang Y X, et al. Evolution of recrystallization microstructure and texture during rapid annealing in strip-cast non-oriented electrical steels. J Magn Magn Mater, 2015, 381: 433–439
60 Liu H T, Li H L, Schneider J, et al. Effects of coiling temperature after hot rolling on microstructure, texture, and magnetic properties of non-oriented electrical steel in strip casting processing route. Steel Res Int, 2016, 87: 1256–1263
61 Song H Y, Liu H T, Lu H H, et al. Fabrication of grain-oriented silicon steel by a novel way: Strip casting process. Mater Lett, 2014, 137: 475–478
62 Wang Y, Xu Y B, Zhang Y X, et al. Development of microstructure and texture in strip casting grain oriented silicon steel. J Magn Magn Mater, 2015, 379: 161–166
63 Fang F, Zhang Y, Lu X, et al. Inhibitor induced secondary recrystallization in thin-gauge grain oriented silicon steel with high permeability. Mater Des, 2016, 105: 398–403
64 Song H Y, Liu H T, Liu W Q, et al. Effects of two-stage cold rolling schedule on microstructure and texture evolution of strip casting grain-oriented silicon steel with extra-low carbon. Metall Mat Trans A, 2016, 47: 1770–1781
65 Song H Y, Liu H T, Lu H H, et al. Effect of hot rolling reduction on microstructure, texture and ductility of strip-cast grain-oriented silicon steel with different solidification structures. Mater Sci Eng-A, 2014, 605: 260–269
66 Song H Y, Lu H H, Liu H T, et al. Microstructure and texture of strip cast grain-oriented silicon steel after symmetrical and asymmetrical hot rolling. Steel Res Int, 2014, 85: 1477–1482
67 Song H Y, Liu H T, Wang Y P, et al. Microstructure and texture evolution of ultra-thin grain-oriented silicon steel sheet fabricated using strip casting and three-stage cold rolling method. J Magn Magn Mater, 2017, 426: 32–39
68 Wang Y P, Liu H T, Song H Y, et al. Ultra-thin grain-oriented silicon steel sheet fabricated by a novel way: Twin-roll strip casting and two-stage cold rolling. J Magn Magn Mater, 2018, 452: 288–296
69 Fang F, Lu X, Zhang Y X, et al. Influence of cold rolling direction on texture, inhibitor and magnetic properties in strip-cast grain-oriented 3% silicon steel. J Magn Magn Mater, 2017, 424: 339–346
70 Fang F, Lu X, Lan M, et al. Effect of rolling temperature on the microstructure, texture, and magnetic properties of strip-cast grain-oriented 3% Si steel. J Mater Sci, 2018, 53: 9217–9231
71 Wang Y, Xu Y B, Zhang Y X, et al. Effect of annealing after strip casting on texture development in grain oriented silicon steel produced by twin roll casting. Mater Charact, 2015, 107: 79–84
72 Fang F, Lan M F, Lu X, et al. The impact of niobium on the microstructure, texture and magnetic properties of strip-cast grain oriented silicon steel. J Magn Magn Mater, 2017, 442: 1–7
73 Lu X, Xu Y B, Fang F, et al. Characterization of microstructure and texture in grain-oriented high silicon steel by strip casting. Acta Metall Sin (Engl Lett), 2015, 28: 1394–1402
74 Lu X, Xu Y, Fang F, et al. Microstructure, texture and precipitate of grain-oriented 4.5wt% Si steel by strip casting. J Magn Magn Mater, 2016, 404: 230–237
75 Lu X, Fang F, Zhang Y X, et al. Microstructure and magnetic properties of strip-cast grain-oriented 4.5%Si steel under isochronal and isothermal secondary annealing. J Mater Sci, 2017, 53: 2928–2941
76 Lu X, Fang F, Zhang Y X, et al. Evolution of microstructure and texture in grain-oriented 6.5%Si steel processed by strip-casting. Mater Charact, 2017, 126: 125–134
77 Kuziak R, Kawalla R, Waengler S. Advanced high strength steels for automotive industry. Arch Civil Mech Eng, 2008, 8: 103–117
78 Xiong Z P, Kostryzhev A G, Stanford N E, et al. Microstructures and mechanical properties of dual phase steel produced by laboratory simulated strip casting. Mater Des, 2015, 88: 537–549
79 Xiong Z P, Kostryzhev A G, Stanford N E, et al. Effect of deformation on microstructure and mechanical properties of dual phase steel produced via strip casting simulation. Mater Sci Eng-A, 2016, 651: 291–305
80 Xiong Z P, Saleh A A, Kostryzhev A G, et al. Strain-induced ferrite formation and its effect on mechanical properties of a dual phase steel produced using laboratory simulated strip casting. J Alloys Compd, 2017, 721: 291–306
81 Xiong Z, Kostryzhev A G, Zhao Y, et al. Microstructure evolution during the production of dual phase and transformation induced plasticity steels using modified strip casting simulated in the laboratory. Metals, 2019, 9: 449
82 Wang H, Yuan G, Kang J, et al. Microstructural evolution and mechanical properties of dual phase steel produced by strip casting. Mater Sci Eng-A, 2017, 703: 486–495
83 Xiong Z P, Kostryzhev A G, Saleh A A, et al. Microstructures and mechanical properties of TRIP steel produced by strip casting simulated in the laboratory. Mater Sci Eng-A, 2016, 664: 26–42

84 Xiong Z P, Kostryzhev A G, Chen L, et al. Microstructure and mechanical properties of strip cast TRIP steel subjected to thermo-mechanical simulation. Mater Sci Eng-A, 2016, 677: 356–366
85 Wang H S, Yuan G, Zhang Y X, et al. Microstructural evolution and mechanical properties of duplex TRIP steel produced by strip casting. Mater Sci Eng-A, 2017, 692: 43–52
86 Xiong Z P, Saleh A A, Marceau R K W, et al. Site-specific atomic-scale characterisation of retained austenite in a strip cast TRIP steel. Acta Mater, 2017, 134: 1–15
87 Daamen M, Wietbrock B, Richter S, et al. Strip casting of a high-manganese steel (FeMn22C0.6) compared with a process chain consisting of ingot casting and hot forming. Steel Res Int, 2011, 82: 70–75
88 Daamen M, Nessen W, Pinard P T, et al. Deformation Behavior of High-manganese TWIP steels produced by twin-roll strip casting. Procedia Eng, 2014, 81: 1535–1540
89 Daamen M, Haase C, Dierdorf J, et al. Twin-roll strip casting: A competitive alternative for the production of high-manganese steels with advanced mechanical properties. Mater Sci Eng-A, 2015, 627: 72–81
90 Song C, Lu W, Xie K, et al. Microstructure and mechanical properties of sub-rapidly solidified Fe-18 wt%Mn-C alloy strip. Mater Sci Eng-A, 2014, 610: 145–153
91 Yang Y, Zhang J, Hu C, et al. Structures and properties of Fe-(8-16) Mn-9Al-0.8C low density steel made by a centrifugal casting in near-rapid solidification. Mater Sci Eng-A, 2019, 748: 74–84
92 Wang H, Zhang Y, Ran R, et al. A medium-Mn steel processed by novel twin-roll strip casting route. Mater Sci Tech, 2019, 35: 1227–1238
93 Wang Z, Carpenter K, Chen Z, et al. The effect of cooling rate and coiling temperature on the niobium retention in Ultra-Thin Cast Strip steel. Mater Sci Eng-A, 2017, 700: 234–240
94 Felfer P J, Killmore C R, Williams J G, et al. A quantitative atom probe study of the Nb excess at prior austenite grain boundaries in a Nb microalloyed strip-cast steel. Acta Mater, 2012, 60: 5049–5055
95 Dorin T, Wood K, Taylor A, et al. Effect of coiling treatment on microstructural development and precipitate strengthening of a strip cast steel. Acta Mater, 2016, 115: 167–177
96 Stanford N, Dorin T, Hodgson P D. The effect of Nb micro-alloying on the bainitic phase transformation under strip casting conditions. Metall Mat Trans A, 2018, 49: 1021–1025
97 Dorin T, Wood K, Taylor A, et al. Quantitative examination of carbide and sulphide precipitates in chemically complex steels processed by direct strip casting. Mater Charact, 2016, 112: 259–268
98 Sellamuthu P, Hodgson P, Stanford N. Effect of copper on microstructure, recrystallization and precipitation kinetics in strip cast low carbon steel. Mater Res Express, 2020, 6: 1265j5
99 Sellamuthu P, Stanford N, Hodgson P D. Recrystallization kinetic behavior of copper-bearing strip cast steel. Steel Res Int, 2013, 84: 1273–1280
100 Guan B, Hong S H, Schulz C, et al. The microstructure, antimicrobial properties, and corrosion resistance of Cu-bearing strip cast steel. Adv Eng Mater, 2020, 22: 1901265
101 Wang W, Zhu C, Zeng J, et al. MnS precipitation behavior of high-sulfur microalloyed steel under sub-rapid solidification process. Metall Mater Trans B, 2019, 51: 45–53
102 Grydin O, Gerstein G, Nürnberger F, et al. Twin-roll casting of aluminum-steel clad strips. J Manuf Process, 2013, 15: 501–507
103 Münster D, Zhang B, Hirt G. Processing of clad steel strips consisting of a high manganese and stainless steel pairing produced by twin-roll casting. Steel Res Int, 2017, 88: 1600285
104 Stolbchenko M, Grydin O, Schaper M. Influence of surface roughness on the bonding quality in twin-roll cast clad strip. Mater Manufacturing Processes, 2017, 33: 727–734
105 Grydin O, Stolbchenko M, Schaper M. Deformation zone length and plastic strain in twin-roll casting of strips of Al-Mg-Si alloy. JOM, 2017, 69: 2648–2652
106 Haga T, Tkahashi K, Ikawaand M, et al. Twin roll casting of aluminum alloy strips. J Mater Process Tech, 2004, 153-154: 42–47
107 Sahoo S, Ghosh S. Microstructure evolution of eutectic Al-Cu strips by high-speed twin-roll strip casting process. Appl Phys A, 2015, 121: 45–50
108 Wang H, Zhou L, Zhang Y, et al. Effects of twin-roll casting process parameters on the microstructure and sheet metal forming behavior of 7050 aluminum alloy. J Mater Process Tech, 2016, 233: 186–191
109 Kim M S, Kim S H, Kim H W. Deformation-induced center segregation in twin-roll cast high-Mg Al–Mg strips. Scripta Mater, 2018, 152: 69–73
110 Liu Y, Sun Y, Zhang L, et al. Microstructure and mechanical properties of Al-5Mg-0.8Mn alloys with various contents of Fe and Si cast under near-rapid cooling. Metals, 2017, 7: 428
111 Song R, Harada Y, Kumai S. Influence of cooling rate on primary particle and solute distribution in high-speed twin-roll cast Al-Mn based alloy strip. Mater Trans, 2018, 59: 110–116
112 Al-Helal K, Patel J, Fan Z. Melt conditioning twin roll casting with thermo-mechanical treatment of recycled AA6111 alloy. JOM, 2018, 71: 1714–1721
113 Al-Helal K, Chang I, Patel J B, et al. Thermomechanical treatment of high-shear melt-conditioned twin-roll cast strip of recycled AA5754 alloy. JOM, 2019, 71: 2018–2024
114 He C, Li Y, Li J, et al. Effect of electromagnetic fields on microstructure and mechanical properties of sub-rapid solidification-processed Al-Mg-Si alloy during twin-roll casting. Mater Sci Eng-A, 2019, 766: 138328
115 Xu W, Birbilis N, Sha G, et al. A high-specific-strength and corrosion-resistant magnesium alloy. Nat Mater, 2015, 14: 1229–1235
116 Wang J, Wang L, Guan S, et al. Microstructure and corrosion properties of as sub-rapid solidification Mg-Zn-Y-Nd alloy in dynamic simulated body fluid for vascular stent application. J Mater Sci-Mater Med, 2010, 21: 2001–2008
117 Liang D, Cowley C B. The twin-roll strip casting of magnesium. JOM, 2004, 56: 26–28
118 Yang X, Patel J B, Huang Y, et al. Towards directly formable thin gauge AZ31 Mg alloy sheet production by melt conditioned twin roll casting. Mater Des, 2019, 179: 107887
119 Todaro C J, Easton M A, Qiu D, et al. Grain structure control during metal 3D printing by high-intensity ultrasound. Nat Commun, 2020, 11: 1–9
120 Kun Y, Hanqing X, Yilong D, et al. Mechanical properties and formability of ultrasonic treated twin roll casting magnesium alloy sheet. Rare Metal Mater Eng, 2017, 46: 622–626
121 Sorensen D, Hintsala E, Stevick J, et al. Intrinsic toughness of the bulk-metallic glass Vitreloy 105 measured using micro-cantilever beams. Acta Mater, 2020, 183: 242–248
122 Zhang L, Wu Y, Feng S, et al. Rejuvenated metallic glass strips produced via twin-roll casting. J Mater Sci Tech, 2020, 38: 73–79
123 Seki I, Kimura H, Inoue A. Thermal stability and mechanical properties of $Ti_{47.4}Cu_{42}Zr_{5.3}TM_{5.3}$(TM=Co, Fe) metallic glass sheets prepared by twin-roller casting method. Mater Trans, 2008, 49: 498–501
124 East D, Gibson M A, Liang D, et al. Production and mechanical properties of roll bonded bulk metallic glass/aluminum laminates. Metall Mat Trans A, 2013, 44: 2010–2020
125 Lee K S, Lee Y S. Fabrication of a $Cu_{36}Zr_{48}Al_8Ag_8$ bulk metallic glass sheet by atmosphere-controlled vertical twin roll strip casting. Int J Cast Met Res, 2018, 32: 78–84
126 Xu M, Liu G, Li T, et al. Microstructure characteristics of Ti-43Al alloy during twin-roll strip casting and heat treatment. Trans Nonferrous Met Soc China, 2019, 29: 1017–1025
127 Wang W, Zhu C, Zeng J, et al. Microstructures and Nb-rich precipitation behaviors of inconel 718 superalloy under sub-rapid solidification process. Metall Mater Trans A, 2020, 51: 2306–2317
128 Shao C, Zhao S, Wang X, et al. Architecture of high-strength aluminum-matrix composites processed by a novel microcasting technique. NPG Asia Mater, 2019, 11: 69

129 Huang H, Wang J, Liu W. Mechanical properties and reinforced mechanism of the stainless steel wire mesh-reinforced Al-matrix composite plate fabricated by twin-roll casting. Adv Mech Eng, 2017, 9: 168781401771663
130 Morris J W. Making steel strong and cheap. Nat Mater, 2017, 16: 787–789
131 Bhadeshia H K D H, Edmonds D V. The bainite transformation in a silicon steel. Metall Mater Trans A, 1979, 10: 895–907
132 He B B, Hu B, Yen H W, et al. High dislocation density-induced large ductility in deformed and partitioned steels. Science, 2017, 357: 1029–1032
133 Jiang S, Wang H, Wu Y, et al. Ultrastrong steel via minimal lattice misfit and high-density nanoprecipitation. Nature, 2017, 544: 460–464
134 Ding R, Yao Y, Sun B, et al. Chemical boundary engineering: A new route toward lean, ultrastrong yet ductile steels. Sci Adv, 2020, 6: eaay1430
135 Liu L, Yu Q, Wang Z, et al. Making ultrastrong steel tough by grain-boundary delamination. Science, 2020, 368: 1347–1352
136 Wang Y, Sun J, Jiang T, et al. A low-alloy high-carbon martensite steel with 2.6 GPa tensile strength and good ductility. Acta Mater, 2018, 158: 247–256
137 Wang C, Chang Y, Zhou F, et al. M^3 microstructure control theory and technology of the third-generation automotive steels with high-strength and high ductility (in Chinese). Acta Metall Sin, 2020, 56: 400–410